University of Salford MANCHESTER

DEVELOPMENT OF A NOVEL AND VERSATILE SYNTHESIS FOR A POTENTIALLY THERAPEUTIC DI-ARYL-ALKYLAMINE AND RELATED ANALOGUES

CHRISTOPHER J MURPHY - 00523703

MSC BY RESEARCH

UNIVERISTY OF SALFORD – SCHOOL OF SCIENCE, ENGINEERING AND ENVIRONMENT

Table of Contents

List of figures

List of abbreviations

CCB – calcium channel blocker

KRAS – Kirsten rat sarcoma

GTP – Guanosine-5'-triphosphate

GDP – Guanosine-5'-diphosphate

CRC – Colorectal cancer

PDAC – Pancreatic ductal adenocarcinoma

LUAD – Lung adenocarcinoma

c-MET – mesenchymal-epithelial transition factor

MDCK – Madin-Darby canine kidney

ATP – Adenosine triphosphate

MEK – Mitogen-activated protein kinase

ERK – Extracellular signal-regulated kinase

BHK – Baby Hamster Kidney fibroblast cells

DARA – Direct asymmetric reductive amination

ee – Enantiomeric excess

NFSI – *N*-fluorobenzenesulfonamide

TPP – Triphenyl-phosphonium

PCC – Pyridinium chlorochromate

THF - Tetrahydrofuran

DCM – Dichloromethane

DCE - Dichloroethane

$NaHCO_3$ – Sodium bicarbonate

$MgSO_4$ – Magnesium sulphate

AcOH – Acetic acid

TLC – thin layer chromatography

MVP – Meerwein–Ponndorf–Verley

NMR – Nuclear magnetic resonance

s – singlet

d – doublet

t – triplet

m – multiplet

GCMS – Gas chromatography-mass spectrometry

m/z – mass to charge ratio

IR – infrared spectroscopy

Abstract

Fendiline is an obsolete ion channel inhibitor originally prescribed as an anti-hypertensive medicine. However, recent repurposing has shown promising efficacy towards a range of serious ailments, most notably carcinomas including pancreatic and colon, as well as parasites such as malaria. Research has revealed several valuable bioactivities including inhibition of oncogenic signalling pathways, tumour suppression, as well as effectiveness as a potentiator in combination therapy along with contemporary anticancer and anti-malarial medicines.

The aim of the research conducted in this thesis looked to trial two novel synthetic procedures targeted at generating *R*-fendiline, along with a range of substituted derivatives. Despite unexpected complications arising from the second and third steps, the primary four-step procedure was successfully carried out to completion. Herein two analogues of the target molecule, one of them completely novel to the current synthetic literature, were generated and spectroscopically characterised. A shorter two-step synthesis attempted, however, was deemed unsuccessful despite modification.

1. Background information

1.1 Classification, structure, and biological activity.

N-(1-phenylethyl)-3,3-diphenyl-propylamine, commercially distributed as fendiline, (figure 1), is an obsolete non-selective inhibitor of L-type voltage-gated calcium channels, the location of which can be found inside cardiac, vascular, and smooth muscle cells, as well as the Ca^{2+} messenger protein calmodulin. L-type calcium channel proteins functionality involves mediation of intracellular Ca^{2+} influx, thereby regulating pacemaker potentials and arterial blood pressure across cardiomyocytes. (Ge & Ren, 2009). Calcium channel blockers, (CCBs), classified by their organic structure into one of three groups, phenylalkylamines, including Fendiline, dihydropyridines such as amlodipine or benzothiazepines like verapamil, (Bkaily & Jacques, 2009).

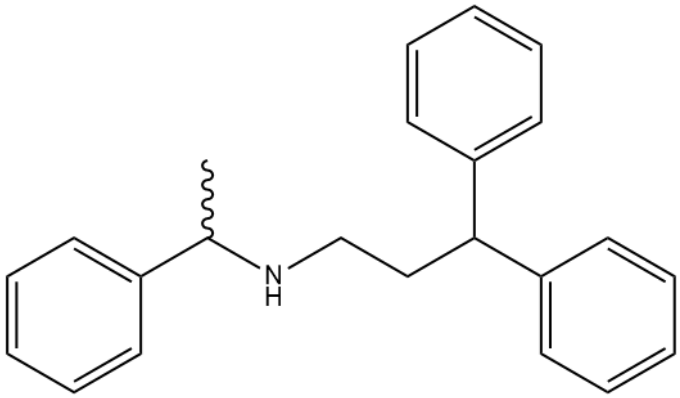

Figure 1 – Structure of racemic fendiline.

The mode of action involves antagonistic binding between the organic molecule and the cell surface channel protein which results in halting of Ca^{2+} ion flux into target cells. This leads to a decrease in intracellular Ca^{2+} concentration, followed by decreased association with the calcium messenger protein, calmodulin. This prevents phosphorylation of the myosin light chain kinase, culminating in relaxation of the smooth muscle tissue and decrease in systolic pressure, (Bayer & Mannhold, 1987). A review by Abernethy & Schwartz, (1999), stated that each classification of CCB has a specific binding site on the channel protein, phenylalkylamines like fendiline bind specifically at motif IV on the α_{1c} subunit, this subunit constitutes the main entry pore unit of the protein. Phenylalkylamines display a low selectivity in their binding action due to their ability to bind to L-type Ca^{2+} channels plus additional ion channels such as Na^{+}/K^{+} and Na^{+}/Ca^{2+}, as well as interactions with more proteins including protein kinase C and plasminogen receptor proteins, (Hockerman, *et al*., 1997; Das *et al.*, 2009; Bkaily & Jacques, 2009).

Physiological outcomes include inhibition of both the sinoatrial, (SA), and atrioventricular, (AV) nodes. Leading to a decrease in heart rate and relaxation of vascular muscles, ensuring vasodilation. These outcomes resulted in fendiline being prescribed for treatment for a range of coronary illnesses as an antianginal/antiarrhythmic medicine as well as treatment for hypertension. While interaction with plasminogen proteins as previously stated also highlighted the drugs anti-inflammatory properties, (Cheng *et al.,* 2001; McDonagh *et al*., 2005).

1.2 Therapeutic repurposing, cancer

Recent research involving fendiline has shed light on the compound's interaction with certain oncogenic cellular pathways. Of these, most notable is the KRAS pathway. This constitutes a group of localised inner-membrane GTPase proteins, which serve as molecular switches to initiate a variety of downstream cell effects including cell proliferation, specialisation, and cell motility. This is done via regulation of nucleotide exchange factors allowing interchange between the active GTP state and inactive GDP state, (Van der Hoeven, 2018; Wang *et al.,* 2021). A review from Zhu *et al.*, (2022), noted KRAS mutations as major oncogenic drivers across several cancers including colo-rectal, (CRC), with between 45-49% of cases in the USA and China containing identifiable mutations. As well as pancreatic ductal adenocarcinoma, (PDAC), has the percentage of cases containing identified mutations reportedly rising to as high as 89-90%. Other notable cancers that express KRAS mutations are shown in figure 2 below. The number of different cancers in which this aberrant pathway is expressed illustrates the potential of reintegration of known compounds that are effective as cell signal pathway inhibitors such as fendiline.

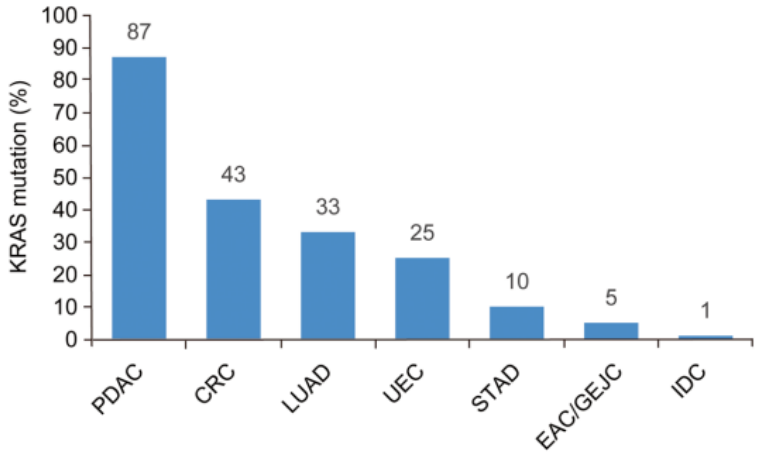

Figure 2 – Graph showing occurrences of detected KRAS mutations in different cancers including pancreatic ductal adenocarcinoma, colorectal carcinoma, lung adenocarcinoma, uterine endometroid carcinoma, stomach adenocarcinoma, oesophageal cancer, and invasive ductal carcinoma, (Zhu *et al.,* 2022).

This was demonstrated in research conducted by Van der Hoeven *et al.*, (2013), had identified that the racemic mixture and *R*-enantiomer of fendiline demonstrated effective mis-localisation of KRAS protein across both MDCK and BHK cell types, reporting IC_{50} values at doses of 9.64 +/- 0.42 µM, all whilst not displaying any significant damage to cell viability. Other observations included recorded inhibition of plasma membrane K-RAS interaction and disruptions to downstream signalling specifically the MEK/ERK pathway.

Examples of repurposing fendiline for cancer are both recent and encouraging. A study by Brizzolara *et al*., (2020) investigated the co-delivery of fendiline hydrochloride alongside established anti-cancer medicine cis-platin to establish any effects on the latter's cytotoxic potential towards in this case, neuroblastoma cells. In vitro analysis found administration of *R*-fendiline leads to inhibition of ATP-binding cassette transporter proteins, which are linked to increased drug resistance and decrease in bioavailability, resulting in increased intracellular cis-platin concentration and cytotoxicity, with the two chemicals described as synergistic in vivo by the authors. Overall, both *in-vitro* and *in-vivo* analysis from neuroblastoma collected from mice, fendiline was demonstrated to increase the anti-tumour ability of cis-platin.

Further evidence of this effectiveness in combination therapy was shown by Alhothali *et al.,* (2019), who researched the combined treatment of PDAC cells with fendiline alongside YAP1 transcription factor inhibitor visudyne and c-MET receptor kinase inhibitor tivantinib. Both play important roles in initiation of certain signalling cascades and upon dysfunction are potent oncogenic factors, (Mo & Liu, 2017; Szulzewsky *et al.,* 2021). A third test group combining fendiline with gemcitabine, a widely used chemotherapy therapeutic was also trialled. Bioassay results found that combination of fendiline with either tivantinib or gemcitabine showed increased cytotoxic and anti-migratory effects across each cell line, while combination with visudyne was effective at higher concentrations, (≥15μM). Other characteristics reported include a reduction in anchorage-Independent growth as well as interference and reduction in self-renewal capability of PDAC cells due to inhibiting the generation of stem-like cells and certain oncogenic cellular signalling processes.

This synergistic relationship demonstrated by fendiline between familiar small molecule inhibitors as well as the recorded inhibitory effects substantiates further investigation and incorporation of the anti-anginal into future oncogenic therapies. Development of a novel synthetic route for fendiline would allow for quick in-house generation of the compound plus a range of analogues that then can be taken and incorporated into bioanalysis and oncogenic screening in further postgrad research.

1.3 Therapeutic repurposing, malaria

Additionally, fendiline has further potential to treat another altogether different malady, malaria. Malaria is caused by five species of protozoan parasites belonging to the plasmodium genus, with transmission occurring through the female anopheles mosquito. Upon infection sporozoite cells accumulate in the host's liver, this accumulation causes hepatocyte cells to burst and release mature merozoite cells into the host's bloodstream, these infect and propagate inside red blood cells, eventually causing said cells to burst and leading to onset of symptoms including flu, muscle aches, jaundice and, if severe, more life-threatening developments like anaemia.

A review published by Jagannathan & Kakuru, 2022, reported that year saw cases of malaria reach approximately 240+ million infected with ~630,00 deaths worldwide. Over 90% of these cases and deaths occurred on the African continent. With anti-malarial resistance been recorded across virtually all current and past anti-malarial therapies, this has compelled anti-malarial research into various directions, each containing obstacles and potential setbacks, (Ippolito *et al.,* 2021), but each also offering an ever developing theranostic understanding of the parasite.

A review by Pandey *et al.,* (2023), noted that many of the traditional strategies utilised against the parasite are proving increasingly ineffective. Methods such as natural product isolation often lead to a very limited number of compounds safe enough to trial effectively, assuming the desired potency isn't lost upon isolation. Derivatisation of already-potent therapeutics can produce a whole new range of biologically active treatments, for example, there are multiple series of derivatives of the well-established anti-malarial chloroquine currently in trials. Despite this potential, the investment required in practical laboratory analysis and financially for organic materials/reagents alone can restrain opportunities for investigation. New drug target identification and/or "omic"-based technology requires a comprehensive understanding and expertise of multiple different parasite biological systems, (genetic, metabolic etc…), and therefore demand extensive resources and time to investigate before any potential treatment may be realistically obtained. Other stratagems such as drug repurposing, resistance-reversal and combinational therapies is where fendiline may hold promising therapeutic potential. At Salford university by M. Rajab in collaboration with Dr. Wilkinson, (2018), reported that the anti-anginal as well as a 2-hydroxy-analogues previously generated by Wilkinson *et al.,* (2007), was biologically active against the highly resistant *Plasmodium falciparum* K1 strain. Combinational studies also found that fendiline was an effective potentiator for established antimalarial Chloroquine.

These examples from both cancer and malarial research indicate a clear potential for fendiline and thereby any potential bioactive analogues to be re-incorporated into future anti-cancer/malarial medicine, either as drug potentiators as demonstrated by Rajab, 2018, or as specifically repurposed medicines. However, with the 2'-hydroxy-analgoues reported increased potency in bioanalysis, this provides compelling evidence for development of a viable and efficient fendiline synthesis which is then capable of manufacturing a range of analogues that may also have medicinal potential.

1.4.1 Previous syntheses & literature review

Previous synthetic work conducted at Salford by Wilkinson *et al.,* (2007), focused on 2-hydroxy-substituted analogues from a 2-hydroxydiphenylmethane starting material with the aim of elucidating the bioactivity of the hydroxy-analogues. The synthetic methodology involved lateral lithiation using *sec*-BuLi thus allowing for nucleophilic substitution with allyl bromide followed by ozonolytic cleavage, then finally reductive amination with *(R/S)*-phenylethylamine chiral reagent to give a corresponding pair of diastereomers indicated in figure 3 below.

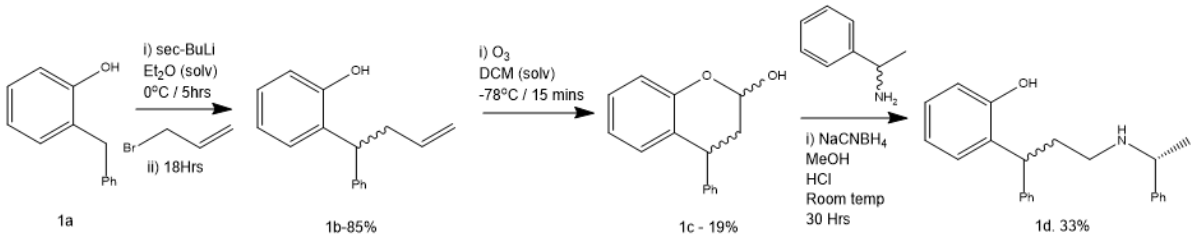

Figure 3 – Reaction scheme presented for synthesis of ortho-hydroxy analogues, (Wilkinson *et al.,* 2007).

Other synthetic procedures for fendiline are also prevalent in the literature. Zheng *et al*., (2016) utilized ferric bromide as a hydrogen-transfer metal catalyst, with deuterium labelling and mechanistic study concluding a Prins-Meerwein–Ponndorf–Verley, (MPV) transfer. Regarding fendiline, starting material, 1,1-di-arylethylene and formaldehyde gave 3,3-diphenylpropanol with a modest 58% yield when scaled up to 2 mmol. Subsequent substitution with tosyl chloride and *N*-alkylation with α-methylbenzylamine at 80°C in a sealed pressure tube gave a very impressive 93% yield for racemic fendiline, (figure 4).

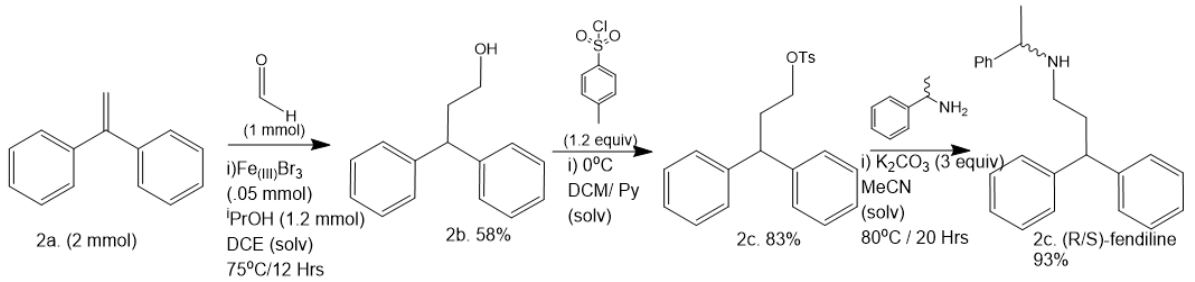

Figure 4 – Schematic for three step synthesis of racemic fendiline from 1,1-diarylethylene by Zhang *et al*., (2016).

Another approach utilised by M. Rajab, (2018), utilised catalytic palladium acetate to facilitate a Heck type coupling, leading to the formation di-phenylpropanal which can then undergo reductive amination with α-methylbenzylamine to give the target fendiline, (figure 5).

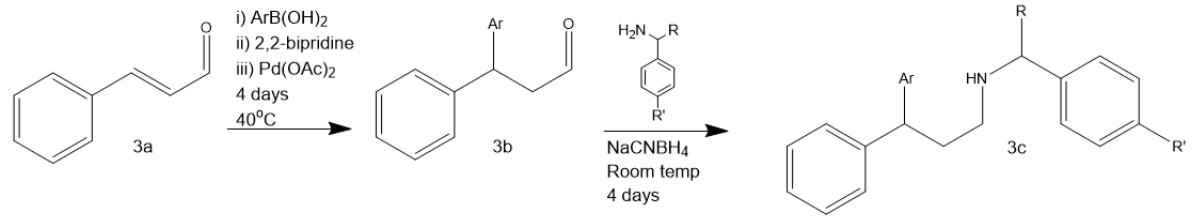

Figure 5 – Schematic for fendiline and analogue synthesis via *trans*-cinammaldehyde via palladium acetate aryl coupling. R = -CH_3, -H. R' = -CH_3, -F, -Cl, -OCH_3, (Rajab, 2018).

Alongside this several analogues were synthesised by utilising a range of substituted amines in the reductive amination step. Meanwhile altering the aryl-boronic reagent opened various synthetic possibilities. Of those attempted, only the diphenyl- and dinaphthyl-aldehyde were feasible. However, the research still demonstrated quick and effective generation of target intermediates while also allowing for the appropriate modifications to the procedure to allow for generation of practical analogues whist maintaining reaction efficacy.

1.4.2 Previous syntheses – Asymmetric reductive amination

Other examples of successful synthesis of the anti-anginal and related analogues are plentiful in the literature, which has given rise to numerous synthetic trends. With one such area of synthetic investigation for fendiline revolves around the direct asymmetric reductive amination, (DARA), step. Asymmetric reduction of imines is extremely important due to the sheer number of *N*-alkyl amine species found in pharmaceutical research as well as concern regarding the appropriate stereoselectivity in the formation of the target amine, (Wakchaure *et al.,* 2015; Huy *et al.,* 2016; Adams *et al.,* 2017; Wu *et al.,* 2022).

Blasius *et al.,* (2020), looked to establish a method for asymmetric reduction of *N*-alkyl imines, by way of a unique in-house synthesised Fe-coordinated bis(oxazolinylmethylidene)isoindoline or "boxmi" heterocycle, (figure 6.2), from which the group had previous success with targeted asymmetric hydroboration of ketones. In combination with pinacolborane, the authors described a method for full asymmetric reduction, reporting *ee*s of >95% across more than a dozen investigated prochiral substates. With these findings rivalling results from pre-established metal catalysts such as iridium and rhodium. Further applicability was shown with the one step asymmetric synthesis of *(R)*-fendiline from *N*-phenylethyliene-diphenylpropylamine. With 0.5 mmol catalyst loading, Blasius *et al.,* (2020) reported very impressive 98% yield with 98% *ee,* (figure 6.1). Thereby successfully developing and demonstrating a novel and facile method of Fe catalysed hydroboration and reduction for bioactive *N*-alkyl targets.

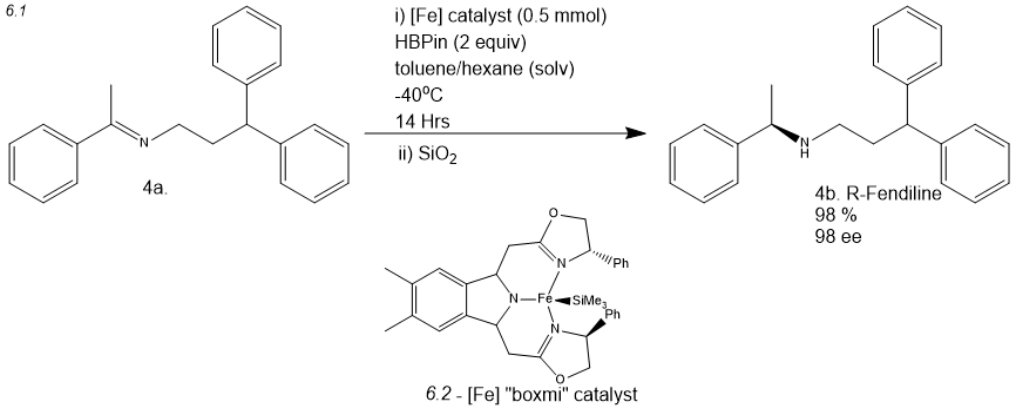

Figure 6.1 – Asymmetric reduction of prochiral imine to (*R)*-fendiline by Blasius *et al.,* (2020). *Figure 6.2* – Skeletal drawing of Fe catalyst.

Another article from Ouyang *et al.,* (2023), utilised an iridium(III) catalyst coupled to a 2-(4,5-dihydro imidazole-2-yl)pyridine, (Pyim), heterocycle, (figure 7). Allowing them to couple together *N*-alkyl amines and carboxylic acids and provide a method for alkyl amine generation meanwhile sidestepping harsh or dangerous conditions/reagents such as borohydride salts or acid-sensitive aldehydes. This demonstrated a high degree of functional group tolerance among over 24 analysed

substrates. *(R)*-fendiline was synthesised in a one-pot method from (*R*)-α-methylbenzylamine and 3,3-diphenylpropanoic acid.

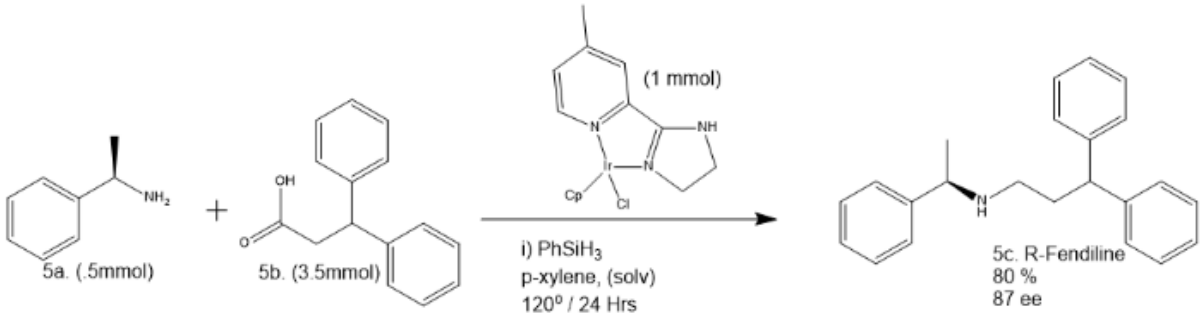

Figure 7 – Schematic for Iridium catalysed reductive amination between (*R*)-α-methylbenzylamine and 3,3-diphenylpropanoic acid.

An article from 2021 by Guo *et al.,* investigated the regioselectivity of the hydroformylation of linear and branched alkenes. This involved synthesis of racemic fendiline via a rhodium metal centre coordinated to two phosphorus-based pincer ligands fixed upon a nanodiamond structure. With the hydroformylation of 1,1-diarylethylene achieved in excellent 93% yield, (figure 8).

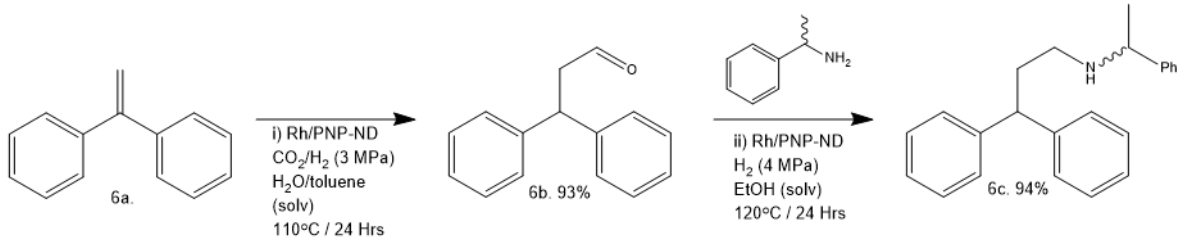

Figure 8 – Reaction scheme for Rh catalysed hydroformylation of 1,1-diphenylethylene followed by reductive amination step to complete synthesis of fendiline racemate by Guo *et al.,* (2021).

1.4.3 Previous synthesis – Related analogues

In the recent synthetic literature, much focus has been on analogues of fendiline. An interesting report by Wang *et al.,* (2021), investigated fendiline exclusively for its binding affinity for KRAS proteins as previously explained in section 1.2 above and in the wider oncological literature. This would help elucidate whether of the chemical structure alterations proposed could vary the binding abilities of fendiline in relation to KRAS cell surface membranes. This resulted in multiple pathways leading to the formation of a range of tertiary fendiline analogues.

Alterations to the original structure as indicated in figure 9, revolved around the forming tertiary amines, with changes also to the diphenyl substructure, intending to increase the hydrophilicity of the molecule, leading to first introducing a double bond at C2-C3 on the propyl chain.

Focus then shifted to forming the tertiary amine formation via a two-step *N*-alkylation procedure. Initial alkylation was accomplished most successfully with reductive amination generating compound 7b. Intermediates 8a-f were synthesised using various alkyl halides. The secondary alkylation step focused on forming a secondary *N,N'*-alkyl/*N'*-cyclic component. Structure-activity relationship, (SAR), testing ultimately concluded a 4-methylpiperazine fragment as the optimal tertiary *N*-chain component, (KRAS mis-localisation assay reported efficacy or E_{max} = 0.75).

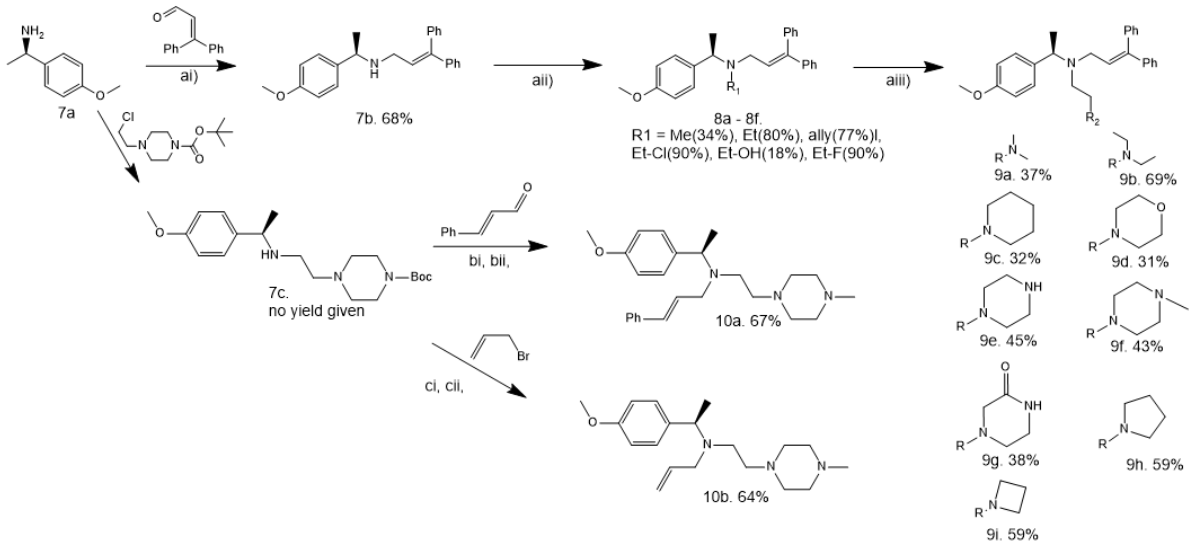

Figure 9 – Synthesis of fendiline analogues 9a-9i and 10a-b generated by Wang *et al.,* (2021).

A second synthetic route was carried out with the *N,N'*-dialkylpiperazine moiety via *N*-alkylation of 7a with tert-butyl 4- (2-chloroethyl)piperazine-1-carboxylate to give intermediate 7c above. This pathway then diverged as the authors looked to replace the hydrophobic diphenyl fragment. Compound 10a was prepared via reductive amination with cinnamaldehyde. The second allyl fragment was introduced via *N*-alkylation of 7c with allyl bromide in combination with potassium carbonate base and a catalytic amount of potassium iodide. Immediate treatment with conc. HCl facilitated removal of the BOC protecting group before a final reductive amination at the piperazine *N'* atom give 10a and 10b.

Another area of investigation included the benzene ring on the starting material *(R)*-α-methylbenzylamine. A new range of analogues was available by substituting different chemical groups at different positions on the benzene ring, (figure 10).

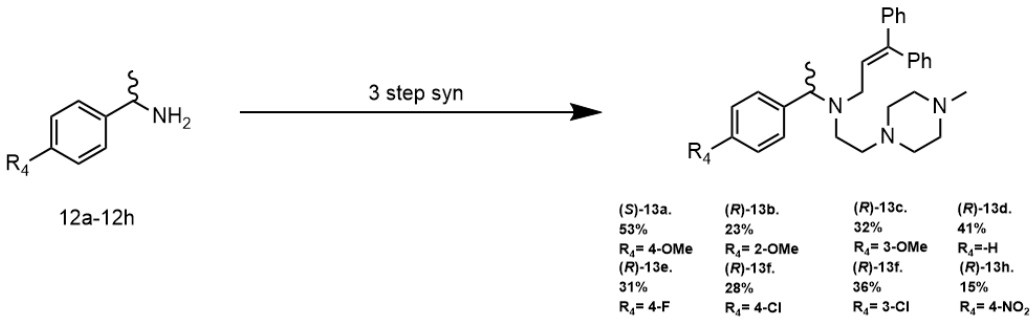

Figure 10 – Scheme for three step conversion of substituted α-methylbenzylamines.

The final synthetic strategy investigated by Wang *et al.,* (2021), focused on the *N*-ethyl piperazine link chain. In the synthesis scheme in figure 11 below, route 5 first shows S_N2 with methylchloroacetate to give 15a. Subsequently the methyl ester intermediate is then saponified to the corresponding carboxylic acid then coupled with an amine.

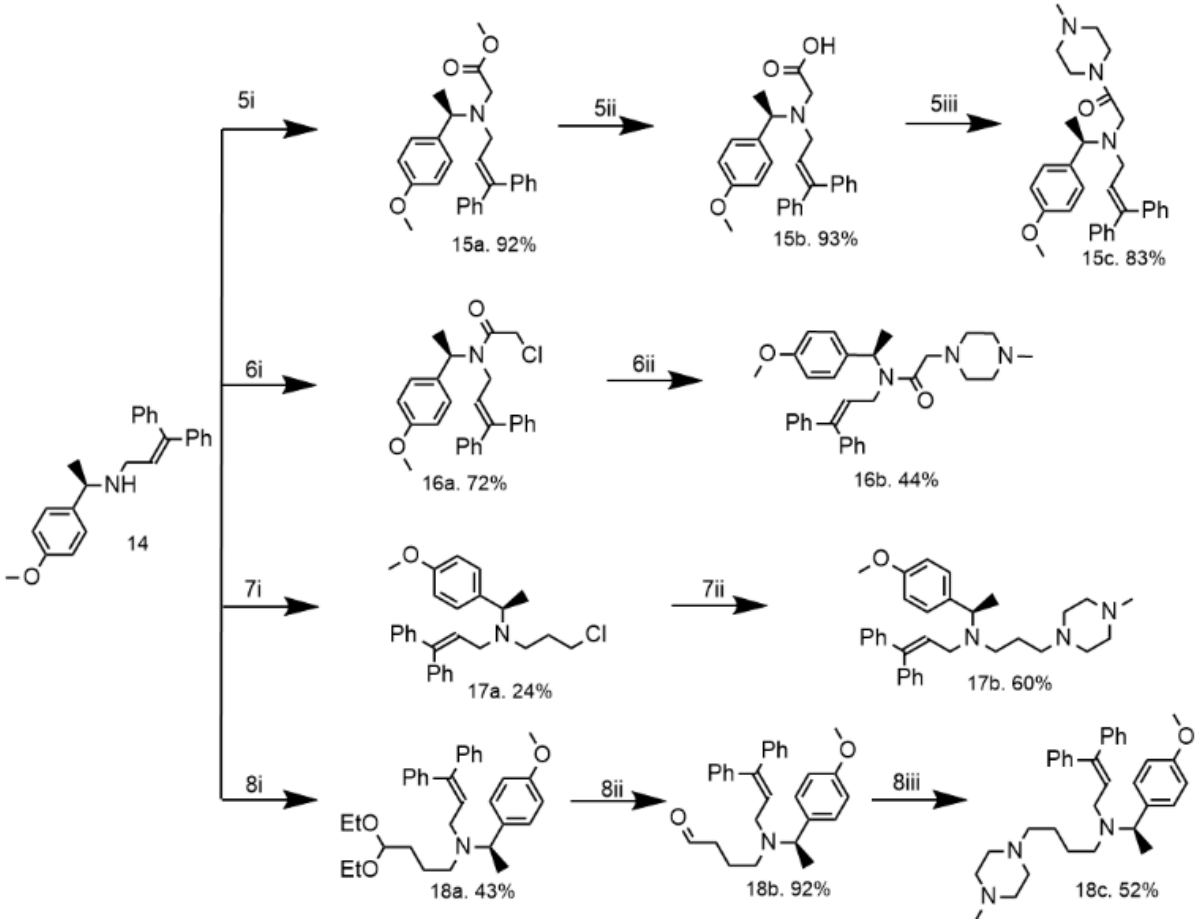

Figure 11 – Reaction schematic for generation of fendiline intermediates and final analogues 15a – 18c by Wang *et al.,* (2021).

Pathway 6 saw 14 undergo a S_N2 with 2-chloroacetyl chloride and a second substitution with N'-methylpiperazine to give compound 16b, (44%). Pathways 7 and 8 looked to increase the length of the piperazine link chain via S_N2 reactions with 1-bromo-3-chloropropane and 4-chlorobutyraldehydediethyl acetal to give compounds 17a, (24%) and 18a, (43%). 18a was then reacted with N'-methylpiperazine, (60%), while 18a's acetal sidechain was deprotected via treatment

with HCl to install a carbonyl on the target chain, (18b - 92%). This butanal sidechain can then react with *N'*-methylpiperazine in a final reductive amination step to give 18c with a moderate 52% yield.

Each intermediate synthesised from figures 19-11, underwent cytotoxicity testing at 30 µM, alongside KRAS mis-localisation assay with gfp-kras g12v expressed in oncogenic MDCK cells. The original bioactive enantiomer *R*-fendiline was incorporated as a reference, (IC_{50} = 0.5 µM, clogP = 9.32). The authors reported intermediate 8d, (IC_{50} = 0.2 µM), showed over double the potency of the fendiline reference. Analogues 9a-i yielded varying results. Heterocyclic structures reported such as Intermediate 9c, gave an IC_{50} of 0.6 µM. Analogue 9f, lead to the highest potency with an IC_{50} of 0.1 µM. Other analogues from this route with decent potency include 9h, (IC_{50} = 0.3 µM), and 9i, (IC_{50} = 0.5 µM).

Analysis of the analogues generated in figure 11 did not show any worthwhile effect on potency or overall efficiency, with the most successful product being analogue 13d, (R = -H, IC_{50} = 0.6 µM). Among the intermediates tested from figure 12 above 17b, containing a propyl-linked *N*-methylpiperazine recored a IC_{50} of 0.1 µM, whist also improving on the partition coefficient, (5.83>5.44), compared to 9f. Overall, this study by Wang *et al.,* (2021) looks to be the most comprehensive recent report into the chemical structure alteration and biological potency of fendiline. Compounds 15c, 16b, 17b and 18c reported in the paper were completely novel to the synthetic literature. This paper highlighted a completely novel methodology in the tertiary derivatisation of fendiline for possible KRAS oncogene treatment and thus increasing the potential scope for further investigation.

A recent trend arising involves introducing fluorine-containing groups into the organic framework. Organofluoro-compound research has increased exponentially, resulting in increasing importance medicinally. Some examples of recorded bioactivities including anti-tumour, (Fluorouracil), anti-microbial, (Levofloxacin) Anti-hypertensive, (Atorvastatin), (Inoue *et al.,* 2020). He *et al.,* (2021) developed a method for efficient and highly enantioselective imine reduction for generating α-trifluoro methylamines, via a binol-derivatised phosphoric acid and a catecholborane as a hydride donor reported ee's up to 96% across a range of substrates, with a 92% ee for *(S)*-α-trifluorobenzylamine. The next step involved removal of the *p*-methoxyphenyl protecting group to allow for the reductive amination step with 3,3-diphenylpropanal and sodium borohydride to give a respectable 69% for the yield for *(S)*-α-trifluoromethyl-fendiline.

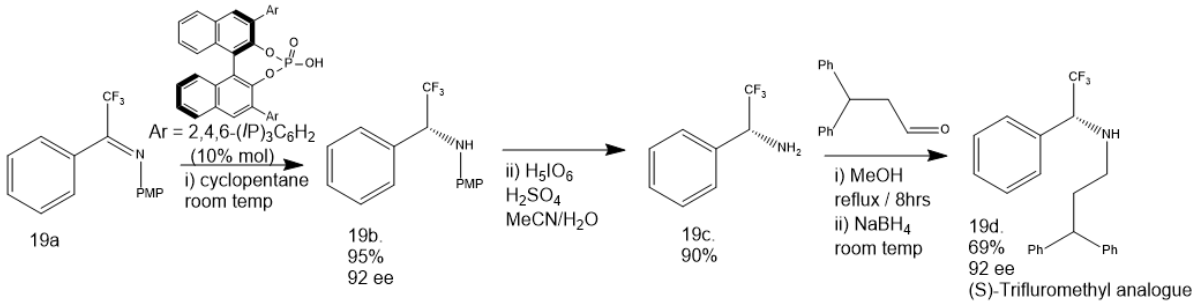

Figure 12 – Synthetic route for synthesis of α-trifluoromethyl-fendiline analogue generated by He *et al.,* (2021).

In another fluoro-based analogue synthesis recorded by Renault *et al.,* (2023), fendiline was among a series of CCBs highlighted when investigating β-fluoro-amine analogues for any stereoelectronic effects observed. This one-pot synthesis involved 3,3-diphenylpropanal reacting with *N*-fluorobenzenesulfonamide, (NFSI), and catalyst *(R)*-5-Benzyl-2,2,3-trimethylimidazolidin-4-one in an

asymmetric β-fluorination step, with diastereoselectivity dictated by which catalytic stereoisomer is preferred. This was then followed by reductive amination shown in figure 13 below.

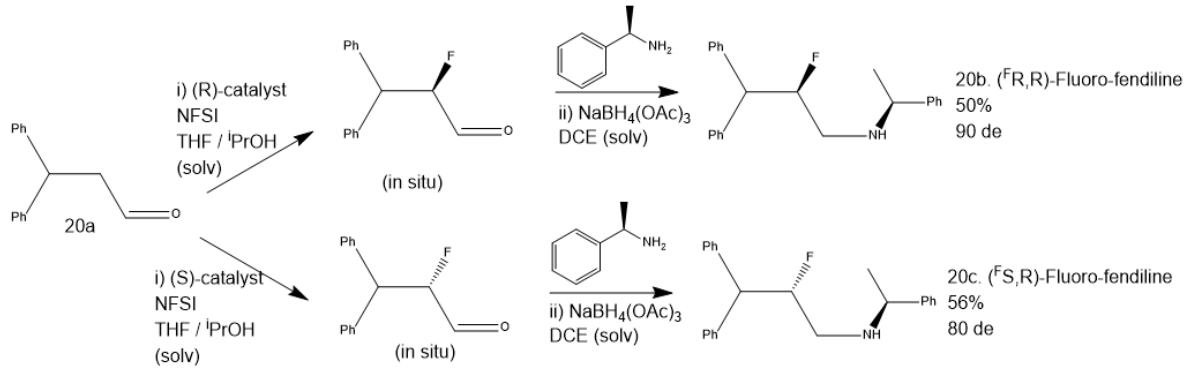

Figure 13 – Schematic route for synthesis of β-fluoro-fendiline diastereomers by Renault *et al.,* (2023).

2 Experimental aims and objectives

The primary aim of this research project was to trial and evaluate a novel short to medium length synthesis route for fendiline and analogues. Upon completion of the procedure the final amine product was fully characterised. Upon completion of the synthesis of fendiline, the process was to be repeated for a series of novel fendiline analogues, starting from 4,4-di-substituted benzophenone derivatives.

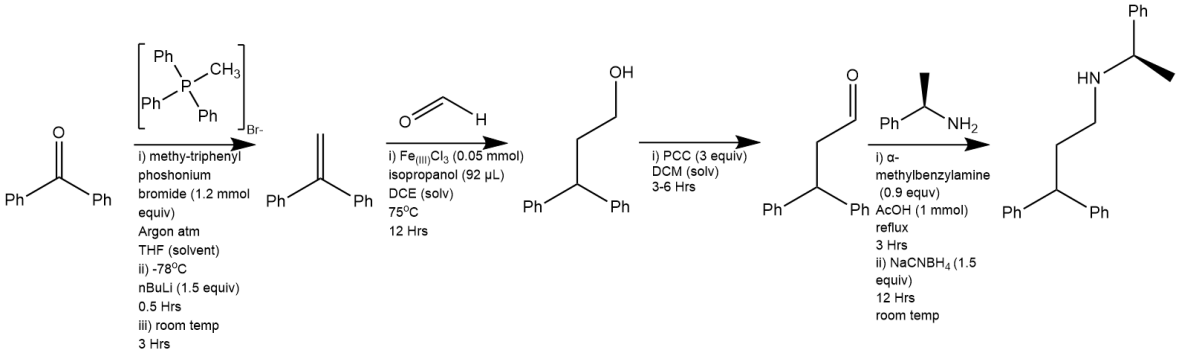

Figure 14 – Reaction scheme for the primary four step synthesis.

Additionally, a second two-step synthesis for a novel 3-pyridinyl-fendiline derivative from 2-benzylpryidine was also to be attempted.

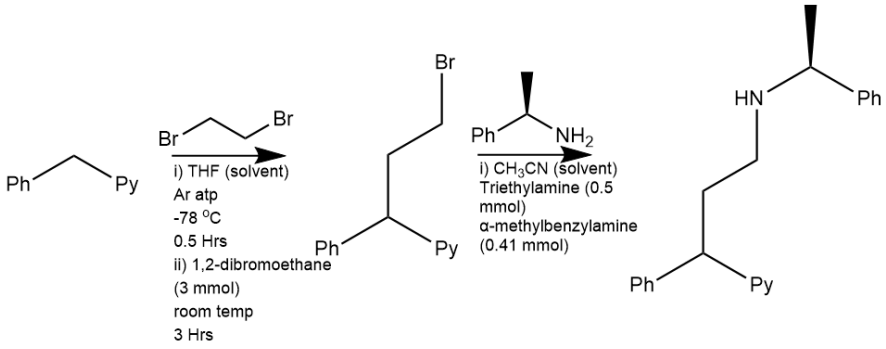

Figure 15 – Reaction scheme for the secondary two step synthesis.

3.Results and discussion

3. 1 Wittig transformation

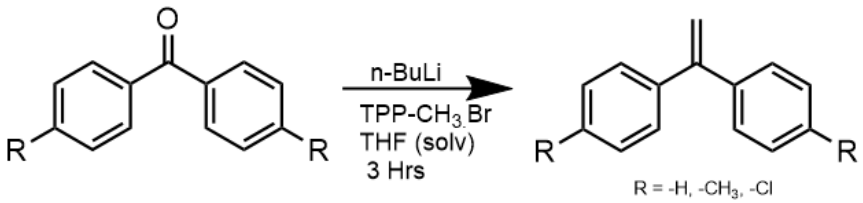

Figure 16 – Scheme for original Wittig transformation with intended alkene product

The first step of the main synthetic route involves the transformation of benzophenone into its ethylene counterpart. The importance of this step stems from the wide range of readily available benzophenone derivatives with different chemical substituents on the di-aryl framework. Any number of symmetrically or asymmetrically substituted benzophenone derivatives could be implemented into the Wittig step highlighting the large degree of versatility, (figure 16). Initial Wittig reactions were conducted with a slight excess of potassium tert-butoxide in anhydrous ether or THF. These first attempts gave moderate yields of 60~65%. Repeats with large excesses of butoxide base did improve final yield somewhat to approx. ~70%, however this raised concerns with solubility issues regarding the large masses of butoxide base to be dissolved. Moreover, TLC analysis of crude products confirmed substantial amounts of unreacted starting material post-reaction.

Upon observing this, the *in-situ* base was changed from butoxide to n-butyllithium. Which in-turn would affect a greater degree of deprotonation of the Wittig reagent and faster rate of formation for the phosphonium ylide. Addition of a slight excess of n-BuLi and leaving to stir for between 15-30 minutes before addition of benzophenone resulted in a much faster reaction step that also requires no dissolving and transferring of base from a separate solution into the reaction mixture. The use of n-BuLi also allowed for the full reaction and purification to be completed the same day and lead to excellent yields of 85-90%. With the range of successful examples generated here, further derivatisation with other non-carbonyl groups such as other longer chain alkyl, ether groups, or asymmetric di-aryl benzophenone starting materials can be confidently integrated into this procedure.

3.2 Microwave assisted Fe coupling.

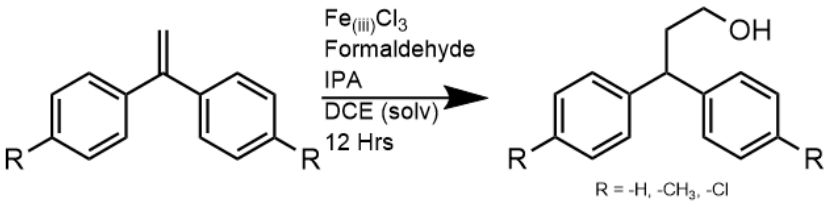

Figure 17 – Scheme for original Fe-mediated alkene-aldehyde coupling with intended alcohol product.

The next synthetic step involved the transformation of the di-aryl alkene into an alcohol, while also extending the main carbon chain from two to three carbons. This was to be done via an alkene/aldehyde coupling reaction previously demonstrated by Zhang *et al.,* (2016). This reaction step involves a mixture of a di-substituted alkene and simple aldehyde in the presence of catalytic Fe(III) salt in dichloroethane, sealed at near boiling point overnight would form a linear propanol intermediate. The method originally employed by the authors, made use of specialised glassware such as pressure tubes to drive forward the reaction. At Salford, alterations to the original method were as follows. First, the use of ferric chloride was chosen over the bromide salt preferred in the original paper. Use of a benchtop microwave reactor to simulate the conditions of a sealed pressure tube would also investigate the effect of microwave heating on the reaction compared to the previous work done by Zhang *et al.,* (2016).

18.1

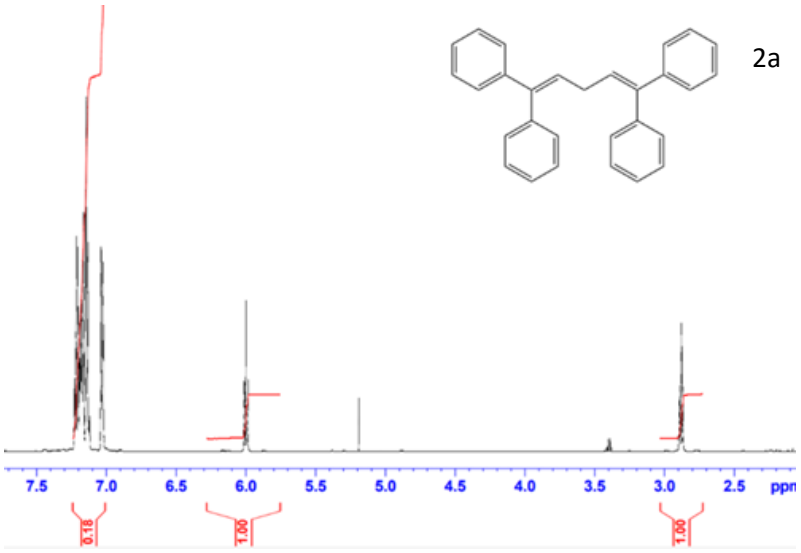

18.2

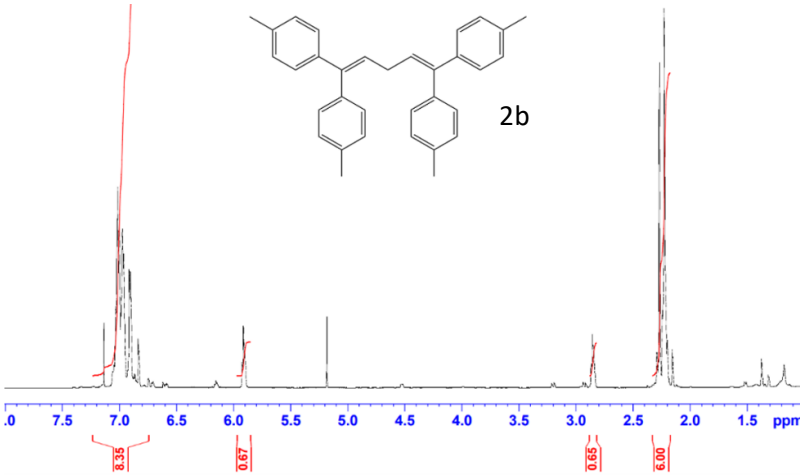

18.3

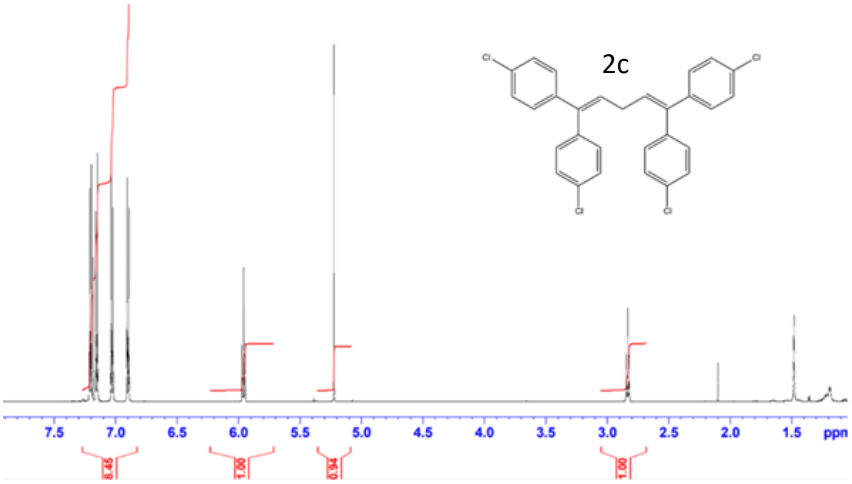

Figure 18.1 – ^{1}H of intermediate 2a. *Figure 18.2* – ^{1}H of intermediate 2b. *Figure 18.3* – ^{1}H of intermediate 2c.

Upon completion and review of the products formed the only major product resolvable by TLC and column chromatography were the tetra-phenyl side-products, 2a-c recorded above. With preliminary spec analysis inconclusive, review of resolvable products included the original reagent alkene and diene coupling product. NMR data of intermediates as shown in figure 18.1-3 above confirmed the major product of the microwave coupling under our conditions to not be the target alcohol. Further analysis of 2a lead to identification of a peak at m/z equal to the molecular ion for the diene product, ($[M]^{+\cdot}$=372). The small lone singlet at ~5.2 was attributed to trace solvent DCE still in the product mixture. Modifications to the procedure included changing the concentration of Iron catalyst to promote association of the reagents with the metal ion centre. Also changing of the length of reaction time, with the side product first theorised to arise due to over-reaction as the length of the reaction progresses.

19.1

19.2

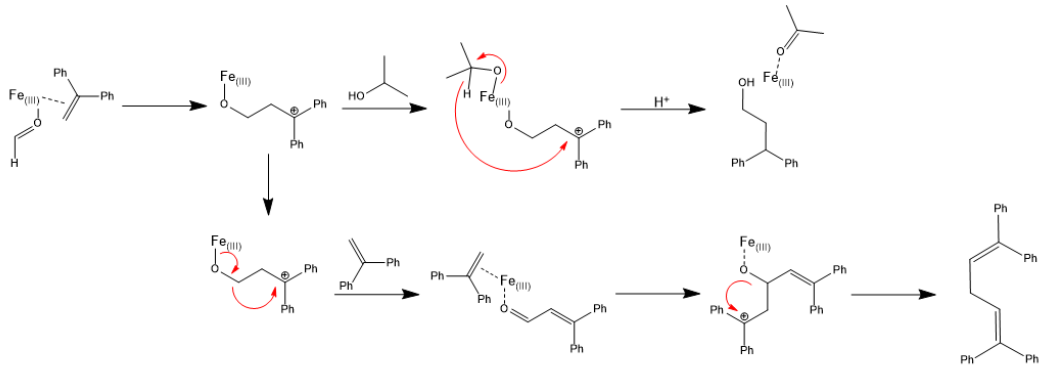

Figure 19.1 – Mechanism for coupling of 1,1-diphenylethylene and formaldehyde via MPV reduction. *Figure 19.2* – Preposed mechanism for formation of diene side-product.

None of the alterations to the method facilitated any meaningful change in the final products yield. Interestingly however, GCMS analysis of the crude mixture did indicate some presence of the deprotonated target alcohol 2a, (([M]$^{+\cdot}$-H^{+})=211), figure 20.1, when referenced against the library database, figure 20.2 below. This was promising enough to moving forward with the synthesis to oxidise the crude mixtures of each intermediate and purifying in the next step.

20.1

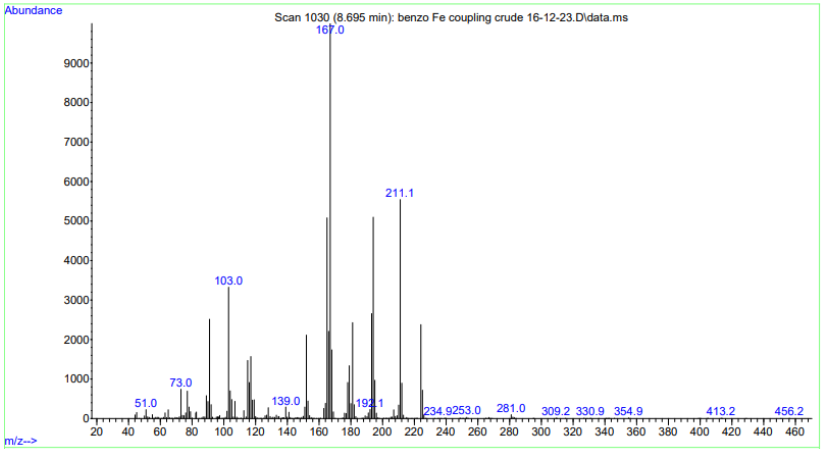

20.2

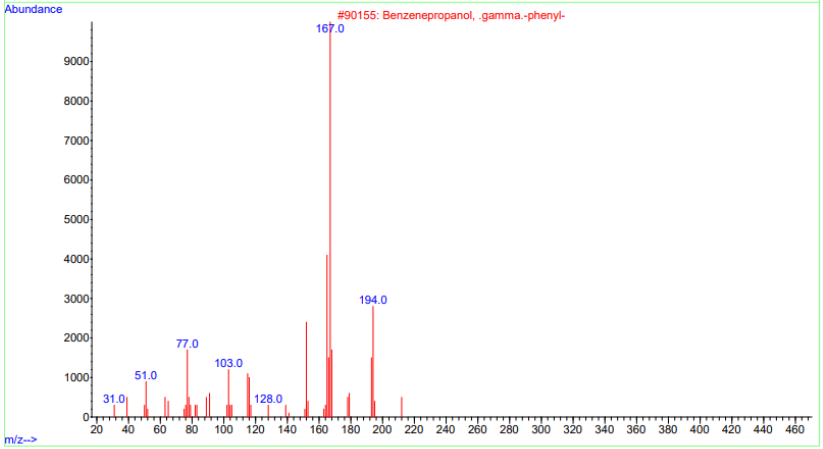

Figure 20.1 – GCMS scan of crude microwave coupling at 8.6 minutes. *Figure 20.2* – Mass spec database reference for 3,3-diphenylpropanol.

The appearance of this side product was unexpected as the original paper made no reference to any major side products forming alongside the target alcohol. However, the changes made to this procedure could help explain how the conditions seemingly preferred over-reaction of 1,1-diaryethylene over the original Fe coupling of di-aryl ethylene and formaldehyde, (figure 19.2). Given the sp^3 carbon sandwiched between both olefin bonds in the pentadiene chain, it can be assumed there is a transition state in which the Fe ion interacts with both the alkene and formaldehyde to increase the original chain length. Zheng *et al.,* (2016), conducted mechanistic analysis and concluded the mechanism was a Prins-MPV type reaction whereby a hydride donor, in this case from isopropanol transfers a hydride ion to the carbocation formed in-situ forming the alcohol before re-entering solution.

The diene functionality at either end of the five-carbon chain suggests that isopropanol couldn't meaningfully affect the reaction mixture. This is critical for the formation of the target alcohol as the isopropanol molecule acts as a hydride donor in the final step of the mechanism, (figure 19.1). A possible outcome of the microwave heating at ~75°C inside the 35 mL reaction tube for up to twelve hours per reaction may have caused the highly volatile co-reagent to separate out from the reaction into a vapor as the reaction progresses. This may explain how only trace amounts of the target

alcohol were synthesised. A possible modification to future procedures may utilise different glassware and seal for the reaction vessel. Smaller glassware may prevent isopropanol vapor forming and keep the hydride donor in solution. Extended heating to the plastic seal for the reaction vessel could damage or warp the seal so that vaporised isopropanol may escape resulting in premature end to the desired coupling reaction.

In the original conditions recorded for the 2 mmol scale reaction producing 3,3-diphenylpropanol by Zheng *et al.,* (2016), they used an excess of alkene with respect to formaldehyde, (2:1 molar ratio), and to the hydride donor isopropanol, (2:1.2), during the reaction. A possible outcome from this stoichiometry used in this method may promote over-coupling of the stable tertiary carbocation intermediate formed initially, allowing for rearrangement to reform the alkene bond before any hydride donor may react. Reaction with another ethylene molecule would then generate the tetra-phenyl species. This abnormal pathway is only speculative given that the original paper was able to complete a series of successful couplings across a range of mono- and di-phenyl reagents.

Upon reflection another repeat under contemporary thermal heating may mitigate vaporisation of the isopropanol reagent, (flashpoint = 53°C). Our use of ferric chloride over the bromide salt chosen in the original paper may also have had effect. Change to the molar stoichiometry may promote incorporation of the hydride donor alcohol into the mechanism and therefore lead to a decrease in the generation of the diene side-product and promote the desired reduction step forming the target alcohol.

3.3 Chlorochromate oxidation

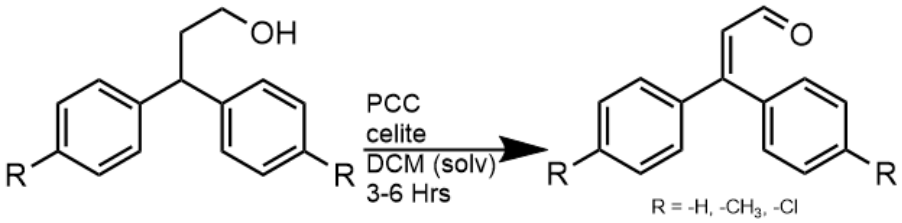

Figure 21 – Scheme for original oxidation procedure via pyridinium chlorochromate, leading to the formation of conjugated aldehyde products.

Oxidation of the crude alcohols made use of ~3 equivalents of pyridinium chlorochromate to drive the reaction to completion and minimise any losses of yield given the observations in the previous step. Despite this, all three oxidation products gave very poor yields ranging from 10-20% with no significant difference in yield arising from the substituent groups. Using 5-10% ethyl acetate in hexane as TLC solvent allowed for the reaction to be monitored until there was no noteworthy change to the new product spot. A colour change was also observed and was helpful as a semi-quantitative guide to reaction progression. Upon addition of chlorochromate reagent, each solution changed from orange to dark yellow for intermediates 3a and 3c, meanwhile di-methyl analogue 3b, underwent a change to dark green. After 3-5 hours each reaction would settle as a dark brown liquid indicative of a complete reaction. Upon isolation of the products however, the αβ-unsaturated isomer of the target aldehydes was seemingly generated. Spectroscopically the presence of an aldehyde is easy to identify with the proton at the carbonyl carbon reporting at >9-10 ppm in ^{1}H NMR. The expected signal pattern would be a triplet at ~9 ppm, followed by a doublet of doublets towards 4~5 ppm caused by the coupling of asymmetric neighbouring environments at C2 on the propyl chain and a triplet signal at approximately 1~2 ppm from the lone proton on the carbon link between the di-phenyl species. However, experimental findings suggest the presence of an alkene bond between C2 and C3. This evidence in figure 22, by the signal pattern. The two doublets at ~9.45 and ~6.51 ppm correlate to the αβ-unsaturated aldehyde product. This was consistent across all three intermediates in the series, supported by database reference standard.

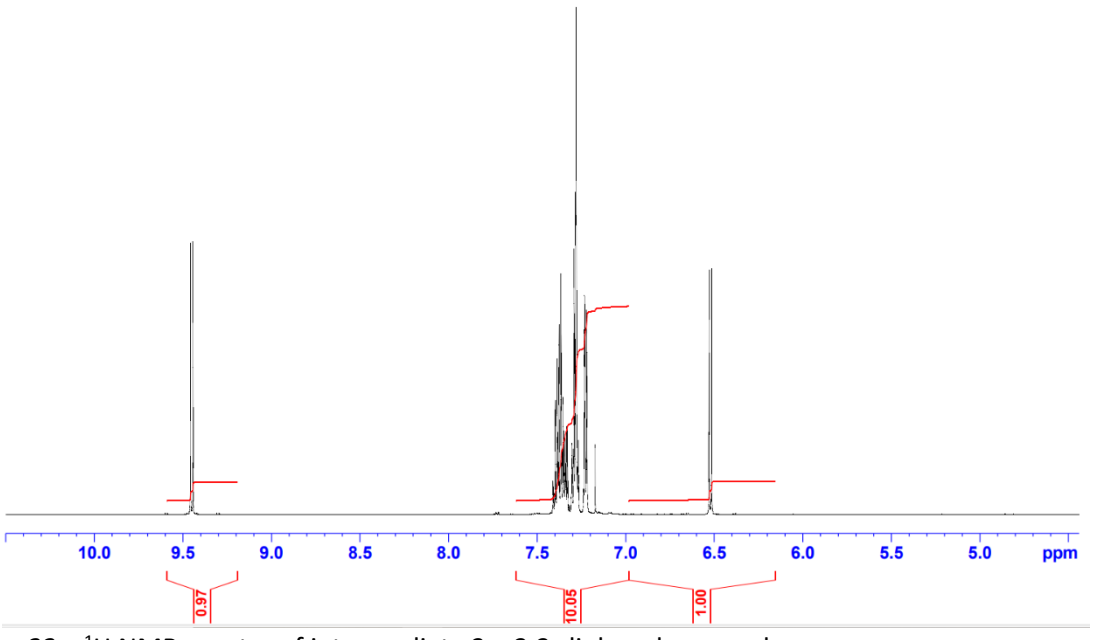

Figure 22 – ^{1}H NMR spectra of intermediate 3a, 3,3-diphenylpropenal.

Carrying out oxidation via pyridinium chlorochromate should not lead to formation of αβ-unsaturated aldehydes as seen here as it is not mechanistically possible, figure 23 below. A reason for these observations may stem from the crude mixtures used from the previous coupling step. Without comprehensive understanding of every possible side product formed, one possibility is that some traces of αβ-unsaturated alcohols may have been generated alongside the saturated alcohol. However, this is unlikely as this would still lead to a mix of 3,3-diphenylpropanal/3,3-diphenylacroaldehyde in each reaction mixture. What may have arisen is the chromate based oxidant may also promote dehydrogenation most likely through any leftover chromium oxide salt generated upon transformation of the alcohol into the aldehyde that isn't immediately removed by the celite bed. Research of Cr oxides as catalysts for dehydrogenation of short-chain alkanes are well documented, (Weckhuysen & Schoonheydt, 1999) with novel research still under investigation, (Monguen *et al.,* 2022). Other effects may include the use of a crude product from the previous step may lead to other undetermined side-reactions.

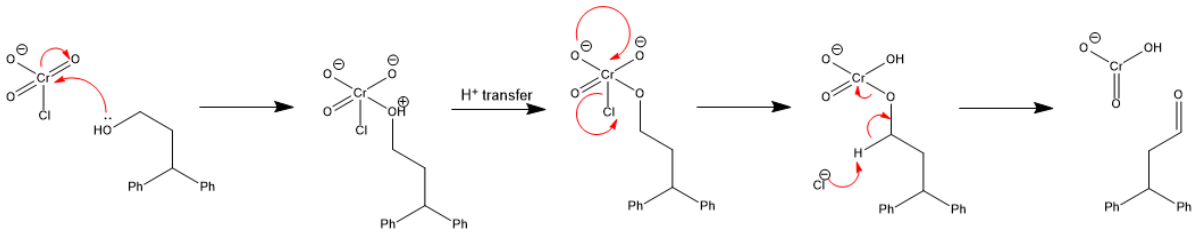

Figure 23 – Mechanism for the oxidation of 3,3-diphenylpropanol to the corresponding aldehyde

24.1

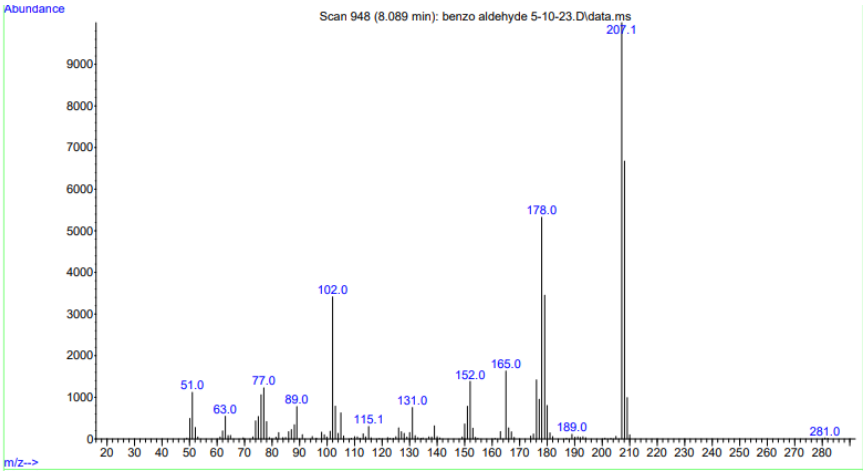

24.2

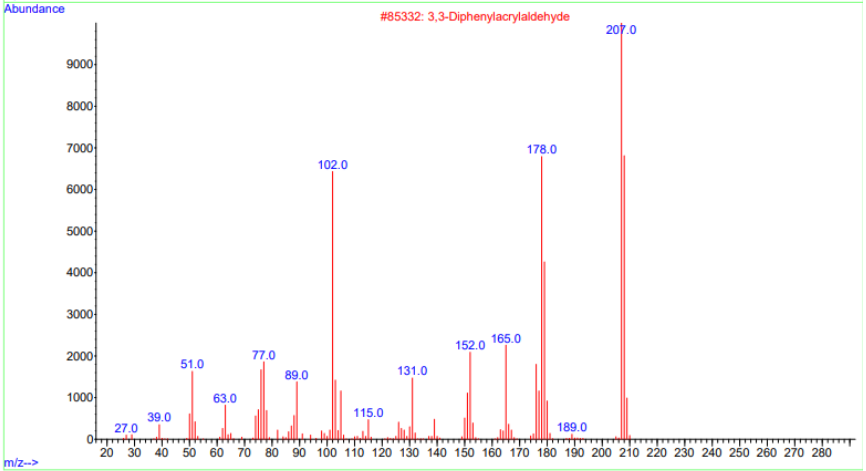

Figure 24.1 – Mass spec of 3a intermediate with. *24.2* – Library reference for diphenylacroaldehyde.

This method if reproducible could be useful in generating a range of conjugated aldehydes without need for separate synthesis of chromium-based dehydrogenation catalysts or specialised catalyst support systems like that of Cr/Al_2O_3, potentially generating a useful one-pot procedure for oxidation/dehydrogenation. Further investigation into the effect of excess celite and equivalents of chlorochromate reagent may elucidate the effect of chromium oxide side-products on the dehydrogenation step in future. Meanwhile changing the oxidising agent to another agent altogether such as Dess-Martin periodinane could achieve selective oxidation from alcohol to the original saturated aldehyde target.

3.4 Reductive amination under reflux

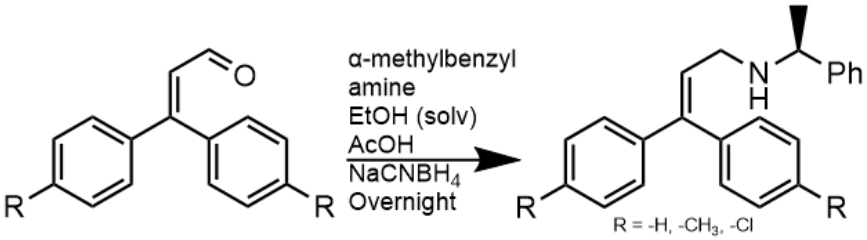

Figure 25 – Scheme for reductive amination of aldehyde intermediate to *R*-dehydro-fendiline via cyanoborohydride salt.

The final step of the pathway involved the reductive amination of the αβ-unsaturated aldehyde intermediates and *(R)*-α-methylbenzylamine to synthesise the dehydro-fendiline. Subsequent synthesis and characterisation of a completely novel 4,4-dimethyl analogue 4b, was carried out, with both final products collected under respectable yields recorded above. From these two successful reactions, I can declare that while the original target fendiline was not synthesised due to unexpected dehydrogenation occurring in the oxidation reaction, this method overall can generate unsaturated fendiline analogues.

Future outlook may look to include an extra reaction step to reduce the alkene bond thus fully synthesising the original fendiline target, and in effect generating another set of potentially biologically active compounds or another possibility could include reaction at the double bond to add other suitable functional groups which may potentiate biological activity.

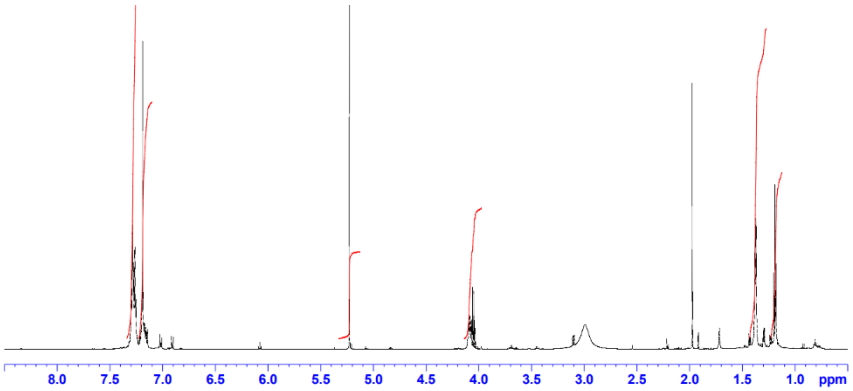

Figure 26 – H^1 NMR spectra of unsuccessful reductive amination step with intermediate 3c.

A 4,4-dichloro analogue was attempted with intermediate 3c, however upon analysis of the final product spectra the reaction was deemed unsuccessful, with both ^{1}H and ^{13}C spectra of the di-chloro analogue not matching that of either of the previous successful reactions. Key to identifying a successful coupling of the amine and aldehyde is a doublet-type peak with an integration ratio of 2H at approximately 3~3.5 ppm, arising due to the $-CH_2$ in-between the amine group and a double

bonded -CH_2. Lack of significant signal in the di-chloro product spectra can confirm the primary attempted coupling of 3c and the chiral amine reagent was unsuccessful.

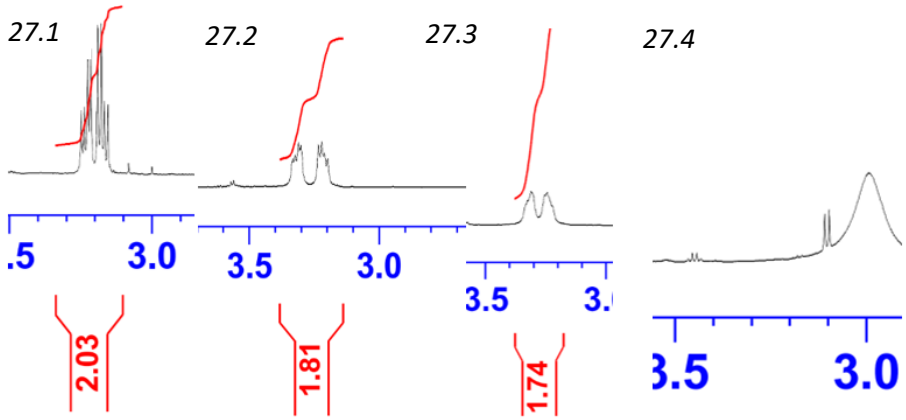

Figure 27.1 – -CH_2 peak for dehydro-fendiline. *Figure 27.2* – -CH_2 peak for dehydro-fendiline re-run. *Figure 27.3* – -CH_2 peak for di-methyl analogue. *Figure 27.4* – Spectrum for di-chloro analogue.

Absence of the triplet peak consistent with 4a/b at 5-6 ppm indicative of the alkene -CH, may indicate the original aldehyde material may have been reduced by excess sodium cyanoborohydride, which may have arisen as a potential negative side effect of the refluxing conditions. Analysis of the di-chloro NMR showed no aldehyde peak at +9 ppm or triplet peak at 5.5-6 ppm. Careful analysis shows two small signals overlapping at around 4 ppm with an integration ratio of ~3. These two signals may represent two of the three carbon environments in the propyl chain for 3,3-Bis(4-chlorophenyl)propan-1-ol, specifically the -CH sandwiched between the di-aryl end of the molecule and the -CH_2 adjacent to the alcohol group. The final -CH_2 multiplet is expected to show up-field. It can be presumed that the messy doublet peak at 1-1.5 ppm is the -CH_3 found on the unused α-methylbenzylamine reactant. The large messy peak at 1.5 ppm could be hiding the remaining carbon environment.

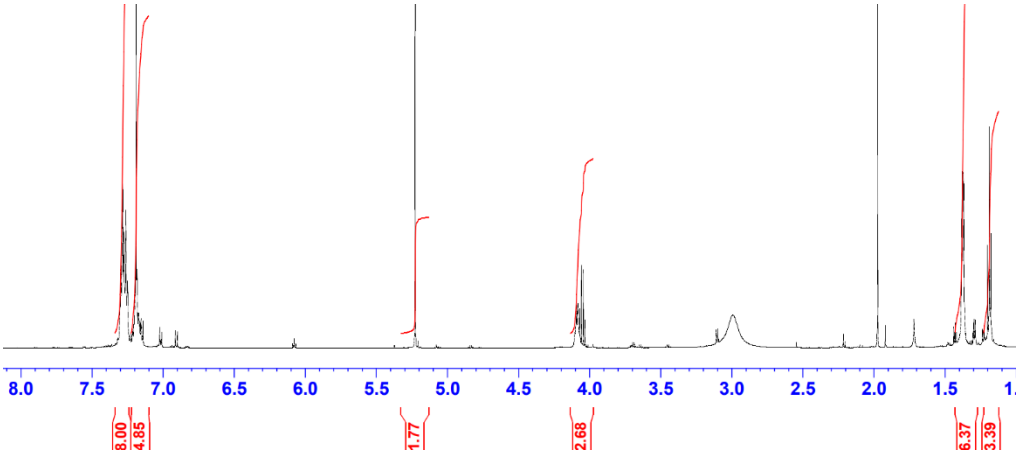

Figure 28 – NMR spectra of attempted reductive amination of intermediate 3c with integration ratios.

While only 2 out of the 3 analogues were successfully synthesised a repeat of the reaction with 3c and a modified molar ratio of reducing agent comparative to the amine/aldehyde reagents or carrying out the procedure below reflux may facilitate the appropriate conversion into the final product

3.5 Alkylation of 2-benzylpyridine

A secondary, shorter synthesis via the use of another di-aryl starting material, 2-benzylpyridine, was also attempted. Due to the wide prevalence and importance of the bi-aryl pharmacophore, substitution of one of the di-aryl groups with a pyridine structure was highlighted as a novel fendiline analogue which may hold potential biological potency and therefore should be investigated.

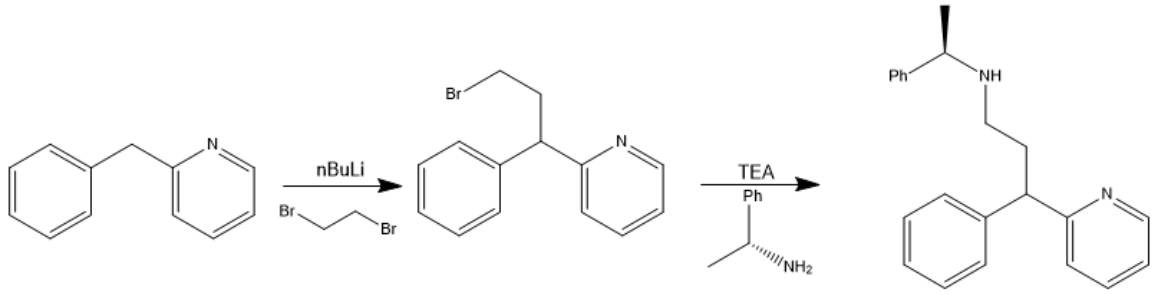

Figure 29 – Original reaction scheme for two-step conversion of 2-benzylpyridine to *R*-fendiline.

The primary step in this next procedure involved lateral lithiation via n-butyllithium, (n-BuLi), to activate the -CH_2 fragment between the aromatics into a carbon nucleophile, facilitating a substitution with 1,2-dibromoethane generating a propyl halide intermediate. Use of a strong base such as n-BuLi was thought to be able to generate the carbon nucleophile species as indicated in figure 30 below, this species could exist in either resonance structure shown below.

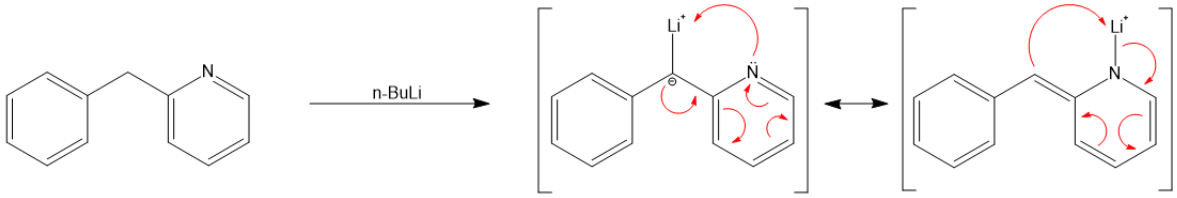

Figure 30 – Diagram of proposed resonance structures of lithiated 2-benzylpyridine reagent.

Unfortunately, the crude NMR spectra, figure 31, indicated no evidence of reaction generating the bromo-intermediate. Modifications including up to three equivalents of the dissolved di-bromoethane, as well as rapid addition of electrophile in anhydrous THF had no observed effect on formation of the target intermediate.

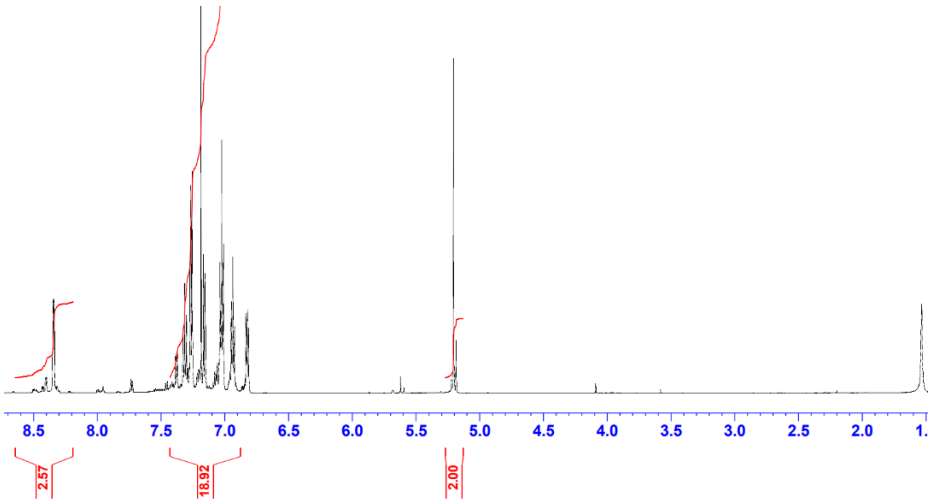

Figure 31 – Crude ^{1}H NMR of attempted alkylation of 2-benzylpyridine with 1,2-dibromoethane.

After continued unsuccessful modifications, the procedure was repeated with a new electrophile 2-chloroethanol, hoping to generate a propanol intermediate like shown in figure 34. However, this attempt was also deemed unsuccessful. Review of the crude NMR, figure 32, shows a small multiplet signal at ~2 ppm which may be indicative of some trace product synthesised, as the characteristic signal for the β-carbon in the propyl-OH target should give a triplet of doublets.

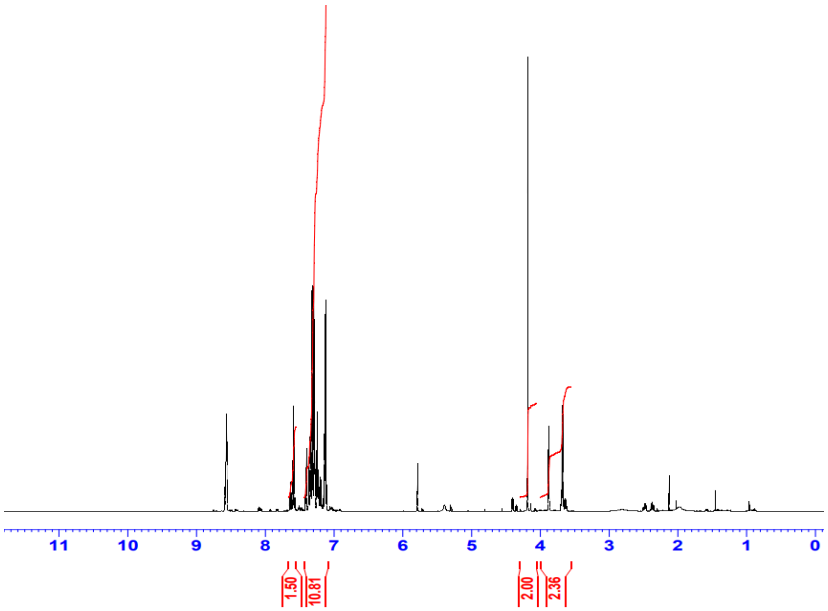

Figure 32 – Crude H^1 NMR of attempted alkylation of 2-benzylpryidine with 2-Chloroethanol.

Given the lack of any clear or prominent product signals in the crude spec analysis, any future adjustments to the procedure could include the use of a more powerful base/lithiating agent, as a possible reason for the complete lack of any trace product may stem from a lack of deprotonation by the n-butyllithium reagent. Literature analysis on reaxys found only one uncited example by Hamid *et al.,* (2009) which utilised n-BuLi and a 2-bromoethanol electrophile, however a written method and results are unlisted.

A stronger base such as *sec*-butyllithium, may fully deprotonate the 2-benzylprydine and thereby facilitate more effective nucleophilic attack. Use of alternate electrophiles such as previously mentioned bromo-alcohol or ethylene oxide which can be effective as a cyclic alkylating agent useable in conjunction with a Lewis acid e.g. $AlCl_3$ to activate the three-membered ring and promote ring opening. Carrying out the addition of butyllithium at a slightly higher temperature like -30°C in a salt and ice bath may promote better reaction between the bromo-alcohol electrophile. Despite this, the overall lack of any meaningful products generated would lead me to conclude this procedure as ineffective and should be disregarded.

4. Experimental

4.1. Wittig via nBuLi

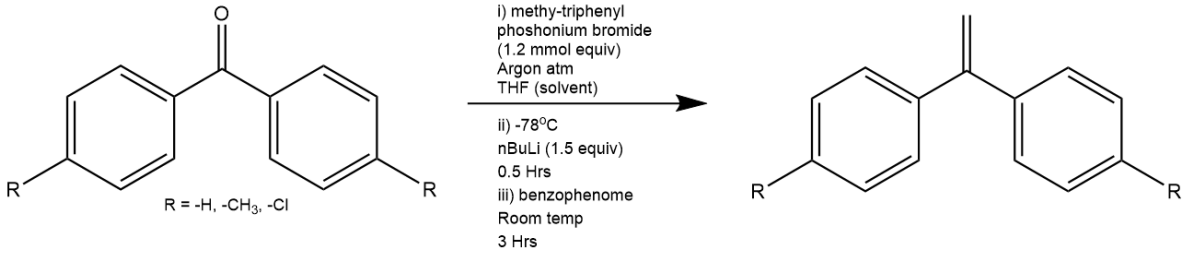

Figure 33 – Reaction scheme for series of Wittig transformations with conditions listed.

To a heat treated round bottom flask, methyl-triphenylphosphonium bromide (0.428 g, 1.2 mmol) flask was added before flushing with argon, followed by addition of anhydrous THF (8 mL). Solution was cooled to -78°C via dry ice/acetone bath followed by addition of n-BuLi (94 µL, 1.6 M, 1.5 mmol), and left to stir for 30 minutes. Then a solution of di-aryl ketone (1 mmol), in THF (2 mL), dropwise to the mixture and then left to stir at room temperature for 3 hours.

Reaction was quenched by addition of isopropyl alcohol (2 mL). Next, dilution with ethyl acetate (20 mL), was followed by washing with sat. $NaHCO_3$(~30 mL), deionised water, (2x30 mL), and brine, (20mL). The organic layer was dried using an excess of $MgSO_4$ then concentrated under reduced pressure to give crude product. Further removal of triphenylphosphine oxide side product was achieved by redissolving solution in hexane/pet ether (5-10 mL) and stirring for 1-2 hours before solution was re-filtered and concentrated. Purification was done via flash silica column chromatography using 100% hexane as the eluent.

1a – 1,1-diphenyethylene (89%) – ^{1}H NMR (600 MHz, $CDCl_3$) δ5.50 (s, 2H), 7.35-7.39 (m, 10H). ^{13}C NMR (600 MHz, $CDCl_3$) δ76.8, 77.0, 77.8, 114.3, 127.7, 128.1, 128.2, 141.5, 150.0.

1b – 1,1-bis(4-methylphenyl)ethene (82%) – ^{1}H NMR (600 MHz, $CDCl_3$) δ2.44(s, 6H), 5.45(s, 2H), 7.20-7.21 (m, 4H), 7.31-7.32 (m, 4H). ^{13}C NMR (600 MHz, $CDCl_3$) δ21.2, 76.8, 77.0, 77.2, 113.0, 128.2, 128.8, 137.4, 138.8.

1c – 1,1-bis(4-chlorophenyl)ethene (85%) – ^{1}H NMR (600 MHz, $CDCl_3$) δ5.35(s, 2H), 7.13-7.16(m, 4H), 7.20-7.22(m, 4H). ^{13}C NMR (600 MHz, $CDCl_3$) δ76.82, 77.04, 77.25, 115.09, 128.50, 129.49, 133.90, 139.49, 147.96.

Intermediates 1a results in accordance with data reported by Yu *et al.,* 2023

Intermediate 1b-c results in accordance with data reported by Mejri *et al.,* 2023

4.2. $FeCl_3$ mediated coupling via microwave heating.

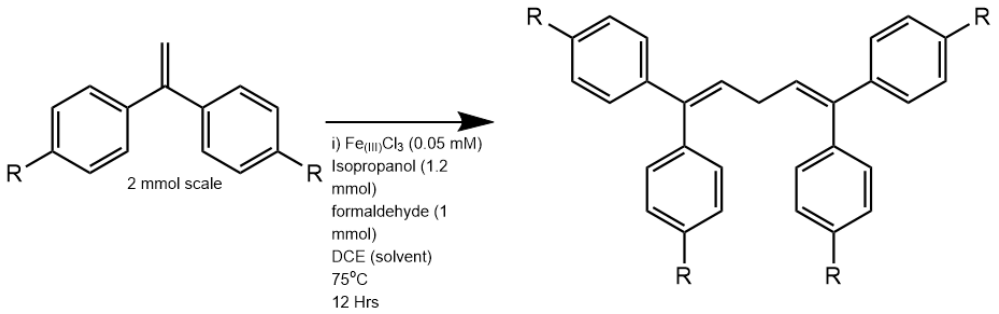

Figure 34 – Reaction scheme for microwave-assisted alkene-aldehyde coupling series.

To a 35 mL glass microwave tube, 1,2-dichloroethane (10 mL), di-aryl alkene (2 mmol), isopropyl alcohol (92 µL, 1.2 mmol), formaldehyde (30 mg, 1 mmol) and ferric chloride (8.1 mg, 0.05 mM) were added. The vessel was sealed, loaded into microwave, and left to stir at 75°C for 12 Hrs.

Post reaction, the sample was diluted with chloroform (30 mL), washed with sat. $NaHCO_3$ (30 mL), deionised water (2x30 mL), then finally brine (20 mL) before drying via using excess $MgSO_4$ then concentration under reduced pressure.

2a – 1,1,5,5-tetraphenyl-1,4-pentadiene (45%) – ^{1}H NMR (600 MHz, CDCl3) δ2.87(t, *J*=7.8 Hz, 2H), 5.99(t, *J*=7.2, 2H), 7.01-7.22(m, 20H). ^{13}C NMR (600 MHz, CDCl3) δ30.67, 76.83, 77.04, 77.25, 126.99, 127.02, 127.27, 127.37, 128.11, 128.18, 129.89, 139.76, 142.29, 142.68.

2b – 1,1,5,5-Tetrakis(4-methylphenyl)-1,4-pentadiene (37%) – ^{1}H NMR (600 MHz, CDCl3) δ2.22(d, J=2.4 Hz 12H), 2.85(m, 2H), 5.91(m, 2H), 6.83-7.13(m, 16H). ^{13}C NMR (600 MHz, CDCl3) δ21.10, 21.26, 30.68, 76.85, 77.06, 77.27, 126.54, 127.31, 128.79, 129.84, 136.42, 136.63, 137.01, 140.20, 141.85.

2c – 1,1,5,5-Tetrakis(4-chlorophenyl)-1,4-pentadiene (48%) – ^{1}H NMR (600 MHz, CDCl3) δ2.83(t, J=7.8, 2H), 5.95(t, J=7.8, 2H). 6.88-7.18(m, 16H). ^{13}C NMR (600 MHz, CDCl3) δ30.52, 76.81, 77.03, 77.24, 127.40, 128.38, 128.53, 128.59, 131.05, 133.25, 133.35, 137.47, 140.42, 140.54.

NMR data for intermediates 2a-c in accordance with data reported by Nishino *et al.,* (1991).

4.3 Oxidation via pyridinium chlorochromate

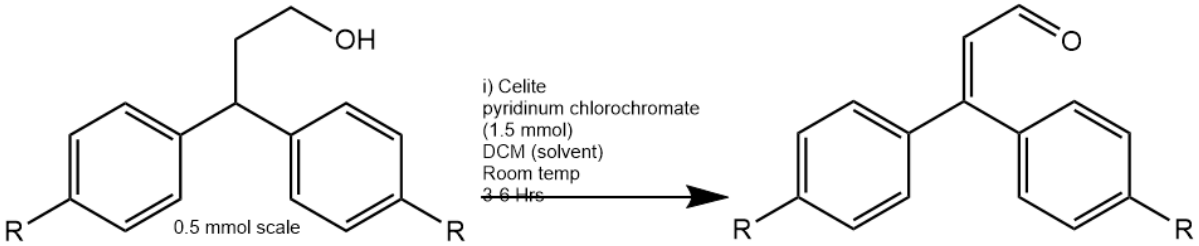

Figure 35 – Reaction scheme for oxidation step by excess pyridinium chlorochromate.

Crude alcohol, (0.5 mmol), was dissolved in DCM (5 mL), then added to a heat-treated round bottom flask. After momentary stirring at room temperature, up to three spatulas of celite powder was added to the flask followed by stirring for 5 minutes before finally adding pyridinium chlorochromate (0.323 g, 1.5 mmol), and left to stir for 3-6 hours. Reaction was monitored via TLC till no further change at starting material spot was observed. Post reaction, the solution was diluted with DCM, (20 mL), filtered through a 2 cm celite/silica filter, then concentrated under reduced pressure.

*Note the formation of an emulsion did occur irregularly in the work-up in which case the mixture was further diluted and washed with excess water (50 mL) and brine (30 mL), in a separatory funnel till no emulsion remained. Mixture was then subsequently dried with excess $MgSO_4$ then concentrated under reduced pressure. Purification was achieved through flash column chromatography via 5-10% ethyl acetate/hexane eluent.

3a – 3,3-Diphenyl-2-propenal (17%) – ^{1}H NMR (600 MHz, CDCl3) δ6.51(d, *J*=7.8 Hz, 1H), 7.21-7.39(m, 10H), 9.44(d, *J*=7.8 Hz, 1H). ^{13}C NMR (600 MHz, $CDCl_3$) δ76.84, 77.05, 77.26, 127.32, 128.36, 128.64, 128.69, 129.46, 130.50, 130.79, 136.72, 139.75, 162.24, 193.48

3b – 3,3-Di(p-tolyl)acrylaldehyde (19%) – ^{1}H NMR (600 MHz, CDCl3) δ2.34(d, *J*=4.2 Hz, 6H), 6.46(d, *J*=7.8 Hz, 1H), 7.08-7.18(m, 8H), 9.42(d, *J*=8.4). ^{13}C NMR (600 MHz, $CDCl_3$) δ21.39, 76.85, 77.06, 77.27, 126.48, 128.77, 128.99, 129.34, 130.84, 133.95, 137.16, 139.62, 140.95, 162.53, 193.70

3c – 3,3-bis(4-Chlorophenyl)acrylaldehyde (13%) – ^{1}H NMR (600 MHz, CDCl3) δ6.47(d, *J*=7.8 Hz, 1H), 7.15.20(m, 4H), 7.27-7.38(m, 4H), 9.42(d, *J*=4.8 Hz, 1H). ^{13}C NMR (600 MHz, $CDCl_3$) δ76.84, 77.05, 77.26, 127.72, 128.90, 129.07, 129.84, 131.96, 134.63, 136.06, 136.98, 137.79, 159.36, 192.62.

NMR data for intermediates 3a-c in accordance with NMR data reported by Bharathi & Periasamy, (1999).

4.4 Reductive amination in refluxing EtOH

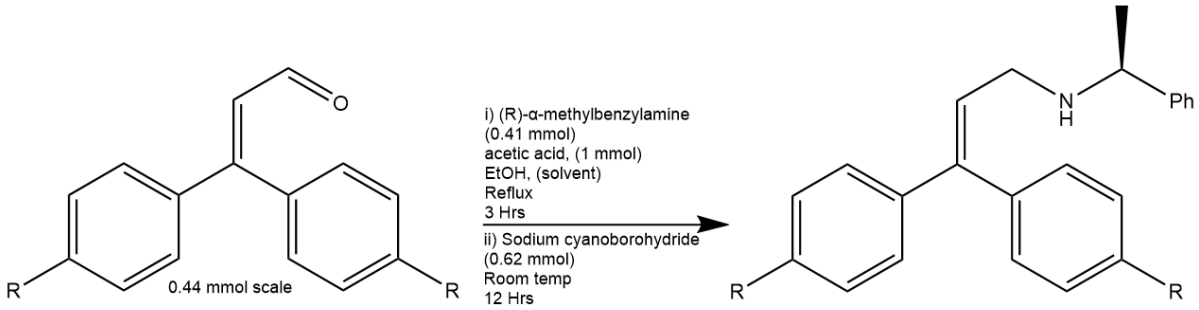

Figure 36 – Reaction scheme for reductive amination under reflux for final amine product.

A solution of (*R*)-α-methylbenzylamine (50 mg, 0.41 mmol, 50 mg) and aldehyde (0.44 mmol) were dissolved in ethanol (4 mL). Then acetic acid (60 µL, 1 mmol), was added dropwise and left to stir for 3 hours under reflux. After 3 hours, reaction was cooled to room temperature before addition of sodium cyanoborohydride (4 mg, 0.62 mmol) and leaving to stir overnight.

Post reaction, the solution was diluted with water (30 mL), ethyl acetate (30 mL), the layers were separated, and the organic layer was washed with 3 M HCl, (3 x 20 mL), the combined aqueous layers were basified with 1 M NaOH to ~9+ pH, then extracted with fresh ethyl acetate. The organic layer was dried with excess $MgSO_4$ and concentrated under reduced pressure to give the final product.

4a – *(R)*-3,3-diphenyl-*N*-(1-phenylethyl)prop-2-en-1-amine (78%) – ^{1}H NMR (600 MHz, CDCl3) δ1.39(d*, J*=6.6 Hz, 3H), 3.15-3.28(m, 2H), 3.81(q*, J*=7.2 Hz, 1H), 6.19(t, *J*=6.6 Hz, 1H), 7.12-7.24(m, 15H) ^{13}C NMR (600 MHz, $CDCl_3$) δ22.76, 45.62, 57.88, 76.84, 77.06, 77.27, 126.07, 127.06, 127.41, 127.53, 127.57, 127.73, 128.15, 128.20, 128.66, 128.72, 129.63, 138.85, 141.66, 145.332. m/z calculated for $C_{23}H_{23}N$ = 313.183, $[M]^{+\cdot}$ = 313.1 . IR: 2888.35, 2979.80, 3656.14.

NMR data in accordance with data reported in by Hancock et al., (2020).

4b – *(R)*-3,3-ditoyl-diphenyl-*N*-(1-phenylethyl)prop-2-en-1-amine (66%) – ^{1}H NMR (600 MHz, CDCl3) δ1.54(d*, J*= 6 Hz, 3H), 2.20(s, 3H), 2.26(s, 3H), 3.24(m, 2H), 3.97(d*, J*= 4.8 Hz, 1H), 6.19(t*, J*= 6 Hz), 6.80-6.98(m, 8H), 7.02-7.04(m, 3H), 7.17-7.20(m, 2H). ^{13}C NMR (600 MHz, $CDCl_3$) δ21.11, 21.20, 57.80, 76.82, 77.03, 77.24, 127.41, 127.53, 128.21, 128.72, 128.84, 128.89, 129.46, 130.20, 135.57, 137.18, 137.18, 137.60, 138.62. m/z calculated for $C_{25}H_{27}N$ = 341.214, $[M]^{+\cdot}$ = 341.1. IR:2663.80, 2929.74, 2888.56, 2979.86, 3656.26

4.5 2-benzyl pyridine – lateral lithiation/alkylation with nBuLi

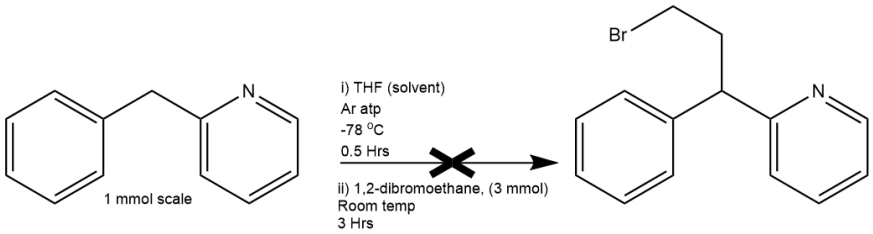

Figure 37 – Reaction scheme for unsuccessful attempt at alkylation of 2-benzylpyridine

2-benzylpryridine, (1 mmol, 0.160 mL), was dissolved in anhydrous THF, (6 mL), inside a heat-treated, argon-flushed multi-neck reaction flask. Reaction was cooled to -78°C with a dry ice/acetone bath followed by addition of nBuLi, (1.6 M, 1.2 mmol, 0.75 mL) dropwise. Then left to stir for up to 30 minutes. Following this, the reaction flask was removed from the dry ice bath followed by dropwise addition of chosen alkylating agent, (3 mmol), dissolved in anhydrous THF, (2 mL). Reaction was left to stir at room temperature for 3 hours.

Upon completion, 2-3 mL of isopropanol was added dropwise to quench, then further diluted with ethyl acetate. Then separated and washed with sat. $NaCO_3$, (30 mL), water, (30 mL), and brine, (20 mL). Organic layer was collected, then dried with an excess of $MgSO_4$ and filtered before finally concentration under reduced pressure to give crude product.

4.6. 2-benzyl pyridine – direct alkylation with α-methylbenzylamine

N/A

5.Conclusions

In conclusion, I have designed and carried out two different synthetic procedures for generating R-Fendiline. The primary four step method took benzophenome and a 4,4-di-methyl derivative to completion and led to the isolation of dehydro-fendiline and a novel 4,4-dimethyl dehydro-fendiline analogue. Despite this success in generating molecules 4a and b, these dehydrogenated analogues of the target amine hereby making the procedure as it is currently only suitable for derivatives with the alkene functionality in mind.

These finding were attributed to an unexpected dehydrogenation occurring in step three causes the key deviation from the target amine rather to the dehydrogenated analogue. These results were identified as major limiting factors in the overall efficiency of the synthesis route. Should this method be re-investigated reconfiguration of the stoichiometry in step two should be considered to investigate the effect on the two identified competing reactions inside the microwave reactor. Furthermore, modification to the choice of oxidiser may facilitate the appropriate carbonyl intermediates without additional side-reactions occurring.

The second synthetic method trialled involved activation of 2-benzylpryidine via *n*-BuLi before alkylation and substitution, however, attempted alkylation was unsuccessful and remained so after repeat. Further alteration to the choice of alkylating agent led to similarly unsuccessful results. Upon reflection a stronger base such as sec-BuLi to better deprotonate the target carbon in-situ, or activation of the electrophile via addition of a Lewis acid may yield improved results.

Bibliography & references

Abernethy, D.R. & Schwartz, J.B. (1999). Calcium-Antagonist Drugs. *The New England Journal of Medicine, 341*(19), 1447-1457. DOI: 10.1056/NEJM199911043411907

Adams, M., Tien, C.H., McDonald, R. & Speed, A. (2017). Asymmetric Imine Hydroboration Catalyzed by Chiral Diazaphospholenes. *Angewandte Chemie, 2017(*56), 16660 –16663. DOI: 10.1002/anie.201709926

Alhothali, M., Mathew, M., Iyer, G., Lawrence, H.R., Yang, S., Chellappan, S., Padmanabhan, J. (2019). Fendiline Enhances the Cytotoxic Effects of Therapeutic Agents on PDAC Cells by Inhibiting Tumor-Promoting Signaling Events: A Potential Strategy to Combat PDAC. *International Journal of Molecular Sciences, 20(*10), 2423. DOI: 10.3390/ijms20102423

Bayer, R & Mannhold, R. (1987). Fendiline: a review of its basic pharmacological and clinical properties. *Pharmatherapeutica, 5*(2), 103-36.

Bharathi, P. & Periasamy, M. (1999). Metalation of Iminium Ions Formed in the Reaction of Tertiary Amines with TiCl4. *Organic Letters, 1*(6), 857-859. DOI: 10.1021/ol990745d

Blasius, C., Heinrich, N., Vasilenko, V. & Gade, L. (2020). Tackling N-Alkyl Imines with 3d Metal Catalysis: Highly Enantioselective Iron-Catalyzed Synthesis of a-Chiral Amines. *Angewandte Chemie, 2023*(59), 15974 – 15977. DOI: 10.1002/anie.202006557

Bkaily, G & Jacques, D. (2009). L-Type Calcium Channel Antagonists and Suppression of Expression of Plasminogen Receptors. *Circulation Research, 2009*(105), 112–113. Doi:10.1161/CIRCRESAHA.109.202028

Brizzolara, A., Garbati, P., Vella, S., Calderoni, M., Quattrone, A., Tonini, G., Capasso, M., Longo, L., Barbieri, R., Florio, T. & Pagano, A. (2020). Co-Administration of Fendiline Hydrochloride Enhances Chemotherapeutic Efficacy of Cisplatin in Neuroblastoma Treatment. *Molecules, 25*(22), 5234-5249. DOI: 10.3390/molecules25225234

Gao, P., Liang, G., Ru, T., Liu, X., Qi, H., Wang, A. & Chen, F.E.(2021). Phosphorus coordinated Rh single-atom sites on nanodiamond as highly regioselective catalyst for hydroformylation of olefins. *Nature Communications, 12*(2021), 4698. DOI: 10.1038/s41467-021-25061-0

Ge, W. & Ren, J. (2009). Combined L-/T-Type Calcium Channel Blockers. *Hypertension, 53,*(4), 592-594. DOI: 10.1161/HYPERTENSIONAHA.108.127548

Hamid, M., Allen, C., Lamb, G., Maxwell, A., Maytum, H., Watson, A. & Williams, J. (2009). Ruthenium-Catalyzed N-Alkylation of Amines and Sulfonamides Using Borrowing Hydrogen Methodology. *Journal of the American Chemical Society, 131*(5), 1766-1774. DOI: 10.1021/ja807323a

Hancock. J., Zhou, J., Van Der Hoeven, D., Frost, J. A., Ye, N. & Wang, P. (2020*). Fendiline Derivatives*. (US 20220177440). US patent Office. US20220177440A1.pdf (storage.googleapis.com)

He, H., Tang, X., Cao, Y. & Antilla, J.C. (2021). Catalytic Asymmetric Reduction of α-Trifluoromethylated Imines with Catecholborane by BINOL-Derived Boro-phosphates. *The Journal of Organic Chemistry, 2021(*86). 4336−4345. DOI: 10.1021/acs.joc.0c03009

Huy, P., Motsch, S. & Kapper, S. (2016). Formamides as Lewis Base Catalysts in SN Reactions—Efficient Transformation of Alcohols into Chlorides, Amines, and Ethers. *Angewandte Chemie, 2016*(55), 10145 –10149. DOI:10.1002/anie.201604921

Inoue, M., Sumii, Y. & Shibata, N. (2020). ontribution of Organofluorine Compounds to Pharmaceuticals. *ACS Omega, 5*(19). 10633-10640 DOI: 10.1021/acsomega.0c00830

Ippolito, M., Moser, K., Kabuya, J.B., Cunningham, C. & Juliano, J. (2021). Antimalarial Drug Resistance and Implications for the WHO Global Technical Strategy. *Current Epidemiology Reports, 2021*(8), 46-62. DOI:10.1007/s40471-021-00266-5

Mejri, E., Higashida, K., Kondo, Y., Nawachi, A., Morimoto, H., Ohshima, T., Sawamura, M. & Shimizu, Y. (2023). Visible-Light-Induced Aminochlorination of Alkenes. *Organic letters, 2*(24), 4581-4585. DOI: 10.1021/acs.orglett.3c01645

Mo, H.N. & Liu, P. (2017). Targeting MET in cancer therapy. *Chronic Diseases and Translational Medicine, 3*(3), 148-153. DOI:10.1016/j.cdtm.2017.06.002

Monguen, C., El Kasmi, A., Arshad, M., Kouotou, P., Daniel, S. & Tian, Z. (2022). Oxidative Dehydrogenation of Propane into Propene over Chromium Oxides. *Industrial & Engineering Chemistry Research, 61*(13). 4546-4560. DOI:10.1021/acs.iecr.2c00813

Nishino, H., Yoshida, T. & Kurosawa, K. (1991). Manganese(III) or Cobalt(III)-Mediated Oxidative Radical Reactions of Terminal Dienes. One-Pot Synthesis of Bis(dihydrofuran)s. *Bulletin of the Chemical Society of Japan, 64*(4). 1097-1107. DOI: 10.1246/bcsj.64.1097

Ouyang, L., Miao, R., Yang, Z. & Luo, R. (2023). Iridium-catalyzed reductive amination of carboxylic acids. *Journal of Catalysis, 418*(2023). 283-289. DOI: 10.1016/j.jcat.2023.01.030

Pandey, S., Anand, U., Siddiqui, W. & Tripathi, R. (2023). Drug Development Strategies for Malaria: With the Hope for New Antimalarial Drug Discovery—An Update. *Advances in medicine, 2023,* article: 5060665. DOI: 10.1155/2023/5060665

Rajab, M. (2018). *Investigating calcium channel blockers as antimalarials* (Publication No…)[PhD thesis, University of Salford]. Available at https://salford-repository.worktribe.com/output/1379840/investigating-calcium-channel-blockers-as-antimalarials

Renault, Y., Diao, J., Cordes, D.B., Leach, K. & O'Hagan, D. (2023). Direct syntheses of stereoisomers of 3-fluoro GABA and βfluoroamine analogues of the calcium receptor (CaR) agonists, cinacalcet, tecalcet, fendiline and NPS R-467. *Medicinal Chemistry Research, 2023*(32). 1532-1542. DOI: 10.1007/s00044-023-03103-0

Szulzewsky, F., Holland, E.C. & Vasioukhim V. (2021). YAP1 and its fusion proteins in cancer initiation, progression and therapeutic resistance. *Developmental Biology , 475*,(2021). DOI: 10.1016/j.ydbio.2020.12.018

Van der hoeven, D., Cho, K.J., Ma, X., Chigurupati, S., Parton, R.G. & Hancock, J.F. (2013). Fendiline Inhibits K-Ras Plasma Membrane Localization and Blocks K-Ras Signal Transmission. *Molecular and Cellular Biology, 33(4)*, 237-251. DOI: 10.1128/MCB.00884-12

Van der hoeven, D., Cho, K.J., Zhou, Y., Ma, X., Chen, W., Naji, A., Montufar-Solis, D., Zuo, Y., Kovar, S., Levental, K., Frost, J., Van der Hoeven, R. & Hancock, J.F. (2018). Sphingomyelin Metabolism Is a Regulator of K-Ras Function. *American Society of Microbiology, 38(3),* Article: e00373-17. DOI: 10.1128/MCB.00373-17

Wang, P., Van der Hoeven, D., Ye, N., Chen, H., Liu, Z., Ma, X., Montufar-Solis, D., Rehl, K., Cho, K., Thapa, S., Van der Hoeven, R., Frost, J., Hancock, J & Zhou, J. (2021). Scaffold repurposing of

fendiline: Identification of potent KRAS plasma membrane localization inhibitors. *European Journal of Medicinal* Chemistry*, 217*(5). Article: 113381. DOI:10.1016/j.ejmech.2021.113381

Wakchaure, V., Kaib, P., Leutzsch, M. & List, B. (2015). Disulfonimide-Catalyzed Asymmetric Reduction of N-Alkyl Imines. *Angewandte Chemie, 2015*(54), 11852 –11856. DOI: 10.1002/anie.201504052

Weckhuysen, B. & Schooneydt, R. (1999). Alkane dehydrogenation over supported chromium oxide catalysts*. Catalysis Today, 51*(2). 223-232. DOI:10.1016/S0920-5861(99)00047-4

Wu, Z., He, H., Chen, M., Zhu, L., Zheng, W., Cao, Y. & Antilla, J. (2022). Asymmetric Reductive Amination with Pinacolborane Catalyzed by Chiral SPINOL Borophosphates. *Organic Letters,24*(51), 9436-9441. DOI:10.1021/acs.orglett.2c03866

Zheng, Y.L., Liu, Y.Y., Wu, Y.M., Wang, Y.X., Lin, Y.T. & Ye, M. (2016). Iron-Catalyzed Regioselective Transfer Hydrogenative Couplings of Unactivated Aldehydes with Simple Alkenes. *Angewandte Chemie, 2016*(55), 6315-6318. DOI: 10.1002/anie.201602130

Yu, J., Liu, T., Sun, W. & Zhang, Y. (2023). Electrochemical Decarboxylative Elimination of Carboxylic Acids to Alkenes. *Organic letters, 25*(43), 7816-7821. DOI: 10.1021/acs.orglett.3c02997

Zhu, C., Guan, X., Zhang, X., Luan, X., Song, Z., Cheng, X., Zhang, W. & Qin, J.J. (2022). Targeting KRAS mutant cancers: from druggable therapy to drug resistance. *Molecular Cancer, 21(159),* DOI: 10.1186/s12943-022-01629-2